Geochemistry, Geophysics, Geosystems

RESEARCH ARTICLE
10.1029/2019GC008586

Key Points:
- Wide-angle seismic and 3D gravity modeling image the deep structure of the Calabrian subduction zone
- The gravity modeling implies that there is no mantle layer between the Calabrian backstop crust and the dipping slab
- Extension of the model using earthquake hypocenters indicates that the slab dip increases abruptly at the Calabrian backstop

Supporting Information:
- Supporting Information S1

Correspondence to:
F. Klingelhoefer,
fklingel@ifremer.fr

Citation:
Dellong, D., Klingelhoefer, F., Dannowski, A., Kopp, H., Murphy, S., Graindorge, D., et al. (2020). Geometry of the Deep Calabrian Subduction (Central Mediterranean Sea) From Wide-Angle Seismic Data and 3-D Gravity Modeling. *Geochemistry, Geophysics, Geosystems*, *21*. https://doi.org/10.1029/2019GC008586

Received 22 JUL 2019
Accepted 31 OCT 2019
Accepted article online 16 NOV 2019

Geometry of the Deep Calabrian Subduction (Central Mediterranean Sea) From Wide-Angle Seismic Data and 3-D Gravity Modeling

David Dellong[1,4], Frauke Klingelhoefer[1], Anke Dannowski[2], Heidrun Kopp[2,3], Shane Murphy[1], David Graindorge[4], Lucia Margheriti[5], Milena Moretti[5], Giovanni Barreca[6], Luciano Scarfì[7], Alina Polonia[8], and Marc-Andre Gutscher[4]

[1]Géosciences Marines, Ifremer, Centre de Brest, Plouzané, France, [2]GEOMAR, Kiel, Germany, [3]Institute for Geosciences, Christian Albrechts University, Kiel, Germany, [4]UMR LGO, University of Western Brittany, Brest, France, [5]Centro Nazionale Terremoti, Istituto Nazionale di Geofisica e Vulcanologia, Rome, Italy, [6]Dipartimento di Scienze Biologiche, Geologiche ed Ambientali, University of Catania, Catania, Italy, [7]Osservatorio Etneo, Istituto Nazionale di Geofisica e Vulcanologia, Catania, Italy, [8]ISMAR CNR, Bologna, Italy

Abstract The Calabrian subduction zone is one of the narrowest arcs on Earth and a key area to understand the geodynamic evolution of the Mediterranean and other marginal seas. Here in the Ionian Sea, the African plate subducts beneath Eurasia. Imaging the boundary between the downgoing slab and the upper plate along the Calabrian subduction zone is important for assessing the potential of the subduction zone to generate megathrust earthquakes and was the main objective of this study. Here we present and analyze the results from a 380-km-long, wide-angle seismic profile spanning the complete subduction zone, from the deep Ionian Basin and the accretionary wedge to NE Sicily, with additional constraints offered by 3-D gravity modeling and the analysis of earthquake hypocenters. The velocity model for the wide-angle seismic profile images thin oceanic crust throughout the basin. The Calabrian backstop extends underneath the accretionary wedge to about 100 km SE of the coast. The seismic model was extended in depth using earthquake hypocenters. The combined results indicate that the slab dip increases abruptly from 2–3° to 60–70° over a distance of ≤50 km underneath the Calabrian backstop. This abrupt steepening is likely related to the rollback geodynamic evolution of the narrow Calabrian slab, which shows great similarity to the shallow and deep geometry of the Gibraltar slab.

Plain Language Abstract We investigate the deep crustal structure of southern Italy and the central Mediterranean where some of the oldest oceanic crust on Earth is actively descending (subducting) into its interior (Speranza et al., 2012). This process causes much of the moderate seismicity observed in this region and may be responsible for strong historical earthquakes as well (Gutscher et al., 2006). Deep seismic data recorded during a marine geophysical expedition performed in 2014 allow us to reconstruct the 3-D geometry of this subduction zone. Our data reveal a 1–4-km-thick evaporitic (salt bearing) layer in the 13-km-thick accretionary wedge. The thin underlying crust has characteristics of oceanic crust. The adjacent onshore domains (E Sicily and SW Calabria) are composed of 25–30-km-thick crust with velocities typical of continental crust. Together with earthquake travel-time tomography (providing images of the subducting slab down to 300 km) and gravity modeling, we can for the first time image the abrupt steepening of the subducting slab, the "slab hinge," where slab dip increases from ≤5° to >60° over a downdip distance of 50 km. This slab dip is steep compared to other subduction zones, for example, in Northern Honshu, Japan, or Sumatra, where the slab dip remains roughly 10°- down to 40-km depth and therefore may have consequences on the seismicity of the region.

1. Introduction

The Calabrian Arc is one of the narrowest subduction zones in the world. Here, the African plate subducts toward the NW beneath the Calabrian and Peloritan continental blocks. The fore-arc region is characterized by moderate seismicity with rare strong events (Carminati et al., 2005; Scarfì et al., 2013). Southern Italy has repeatedly been struck by strong earthquakes that also triggered tsunami (e.g., Messina M7.1 in 1908; Hyblean earthquake M7.5 in 1693—Piatanesi & Tinti, 1998; Jacques et al., 2001; Gutscher et al., 2006).

The seismicity of the slab is distributed along a well-defined Wadati-Benioff zone with focal depth that is less than 50 km in the Ionian Basin and down to 660 km in the Tyrrhenian Basin (Engdahl et al., 1998; Selvaggi & Chiarabba, 1995).

Imaging the boundary between the downgoing slab and the upper plate along the Calabrian subduction zone is important for assessing the potential of a subduction zone to create megathrust earthquakes. Indeed, many authors consider that earthquake rupture cannot extend beyond the intersection with the mantle wedge, which is thought to be highly serpentinized (Byrne et al., 1988; Oleskevich et al., 1999). Other workers have hypothesized that there is a significant influx of hot mantle beneath Calabria (Ferranti et al., 2007; Westaway, 1993), and others evoke slab break-off and possible delamination beneath central E Sicily and Calabria (Faccenna et al., 2011; Giacomuzzi et al., 2012; Piana Agostinetti et al., 2009). However, the exact depth and dip of the downgoing slab, as well as the thickness and nature of the upper plate (Calabria block), remain uncertain. This study tries to unravel the slab geometry and the slab depth in the Calabrian subduction zone using wide-angle seismic data and gravity modeling as well as earthquake locations and regional tomographic data.

1.1. Tectonic History of the Study Region

The evolution of the central western Mediterranean region is driven by the convergence between the African plate and the Iberian and Eurasian plates leading to subduction initiation, slab rollback, and formation of back-arc basins (Faccenna et al., 2011; Handy et al., 2010; Jolivet et al., 2015; Rosenbaum et al., 2002; van Hinsbergen et al., 2014) (Figure 1). NW dipping subduction and ensuing rollback are thought to have started at 35–30 Ma (Rosenbaum et al., 2002; van Hinsbergen, Mensink, et al., 2014). At 25 Ma the Sardinia-Corsica block began rotating in a counterclockwise direction in response to SE-ward retreat of the subduction (Rosenbaum et al., 2002). This led to widespread extension causing the opening of the Liguro-Provencal and Valencia basins (Séranne, 1999). The original forearc then split into individual blocks known as AlKaPeCa (Alboran, Kabylides, Peloritan, Calabria) continental terranes (Bouillin et al., 1986). The Calabrian slab rolled back to the E, and the overriding continental blocks were thrust onto the margin of Adria forming the southern Apennines. The Peloritan block has overthrust the African margin of Sicily (Speranza et al., 2003). A slab length offset between the originally attached Calabrian and the Kabylides slab might be at the origin of the initiation of a subduction-transform edge propagator (STEP, Govers & Wortel, 2005) fault that then separated these into two slabs (van Hinsbergen, Mensink, et al., 2014). The modern-day fore-arc STEP fault is thought to be located either at the Alfeo Fault system (Dellong et al., 2018; Gutscher et al., 2016, 2017) or at the Ionian Fault system (Polonia et al., 2011; Scarfì et al., 2018) (Figure 2). An earlier proposition that the STEP fault follows the Malta Escarpment, a 3-km-high feature offshore E Sicily (Argnani & Bonazzi, 2005) formed during the Tethyan rifting history of the Ionian Sea (Frizon de Lamotte et al., 2011; Gallais et al., 2011), seems unlikely given the absence of tectonic deformation along the central to southern Malta Escarpment since the Messinian, on the basis of high-resolution seismic profiles shot across the escarpment (Gutscher et al., 2016).

1.2. Deep Structure of the Ionian Basin and the Malta Escarpment

Several deep seismic reflection and refraction studies were conducted on the eastern Sicily margin in the 1980s and 1990s (Catalano et al., 2001; Hirn et al., 1997; Makris et al., 1986; Nicolich et al., 2000). These studies concluded that a 30-km-thick continental crust underlies the Sicilian-Hyblean Plateau. An expanding spread profile experiment located in the Ionian Abyssal Plain (IAP) and on the Mediterranean ridge provided the first constraints on the crustal velocities of the deep IAP, where the sedimentary cover is thinnest. The wide-angle seismic results show a 5-km-thick sedimentary cover overlying a thin crust of about 7 to 9 km (de Voogd et al., 1992; Le Meur et al., 1997). However, different interpretations were proposed including a thinned continental crust or an oceanic one. Later studies clearly imaged a 5- to 6-km-thick oceanic crust in the basin spanning the northern IAP (Dannowski et al., 2019; Dellong et al., 2018). Previous multichannel seismic (MCS) studies have imaged the deep structure of the Ionian Basin and the adjacent Calabrian accretionary wedge, with sediment thicknesses increasing from about 5 km (undeformed thickness) in the abyssal plain to 10–15 km within the accretionary wedge as the dip of the subducting plate below remains very shallow (1–2° on average) (Cernobori et al., 1996; Gallais et al., 2011; Maesano et al., 2017; Minelli & Faccenna, 2010; Polonia et al., 2011). An early MCS study imaged the steepening of the subducting basement as it approaches the Calabrian block (lines ION-3 and ION-4) (Cernobori et al., 1996). At the transition

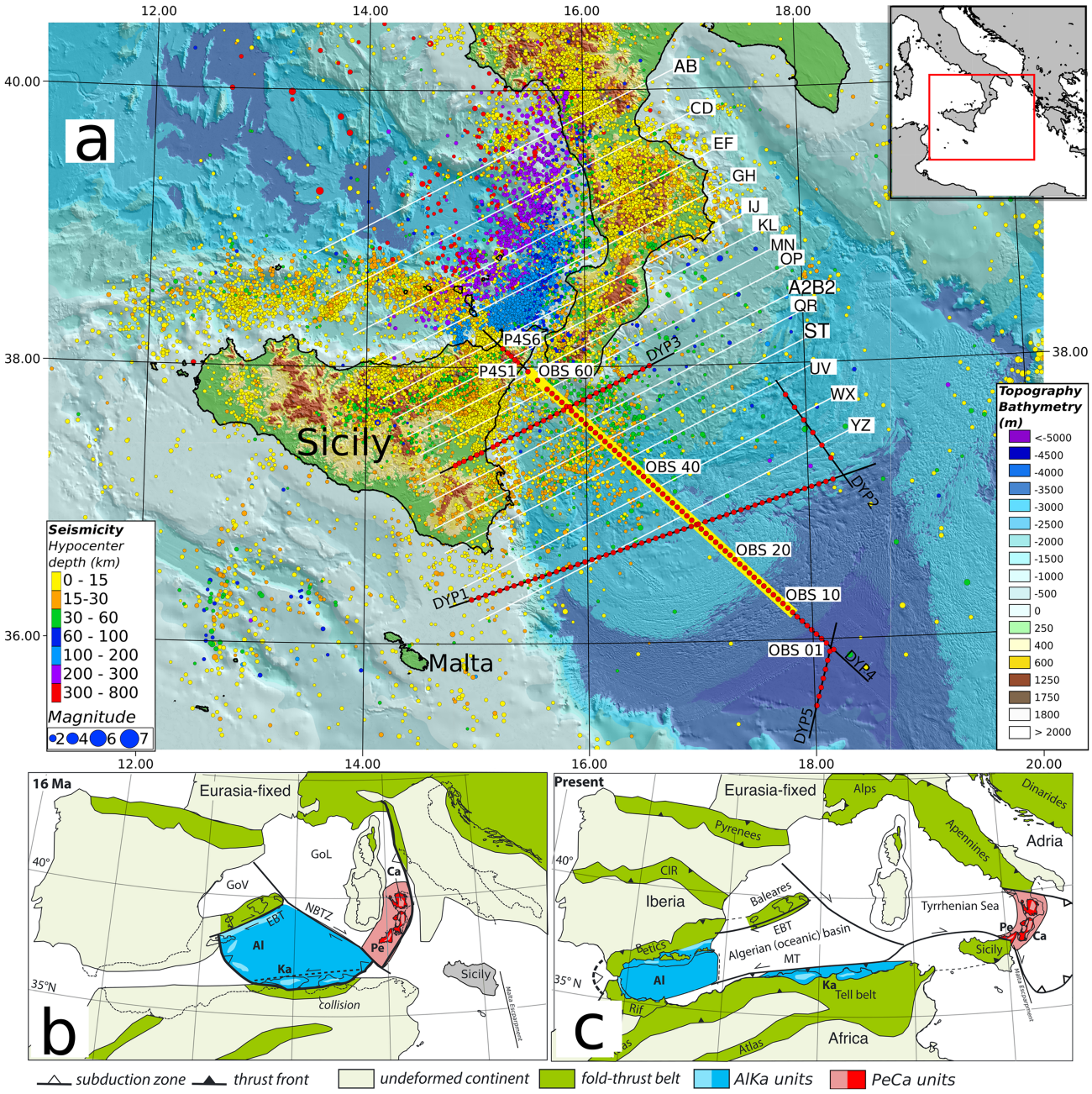

Figure 1. (a) Location map of the study area. Ocean-bottom seismometers and land stations deployed during the Dionysus cruise (October–November 2014, Meteor). Earthquakes from the INGV-ISIDe catalog (http://cnt.rm.ingv.it/en) are plotted with a size proportional to the magnitude and color corresponding to the hypocenter depth. The CROP-M3 MCS profile is coincident with DY-P4 and is marked by underlying bold yellow line (Figure 5 in this study and shown in detail in Polonia et al., 2011). Profiles used for the construction of the gravity model are marked by white lines. Bathymetry from Gutscher et al. (2017) and EMODnet. (b) and (c) Paleogeographic reconstruction figures are modified from van Hinsbergen, Mensink, et al. (2014). Al = Alboran; Ca = Calabria; CIR = Central Iberian Ranges; EBT = Emile Baudot Transform; GoL = Gulf of Lion; GoV = Gulf of Valencia; Ka = Kabylides; NBTZ = North Balearic Transform Zone; Pe = Peloritan Mountains. Inset shows the location of the study is in the central Mediterranean region.

between the continental (Sicilian) and the deep oceanic (Ionian) domain, an abrupt crustal thinning by 3 km is observed along the Malta Escarpment. The escarpment was originally interpreted to be a passive margin originating from the initial opening of the Ionian Sea. Later studies proposed this to be a transform margin (Catalano et al., 2001; Dellong et al., 2018; Frizon de Lamotte et al., 2011; Gallais et al., 2011), which is in

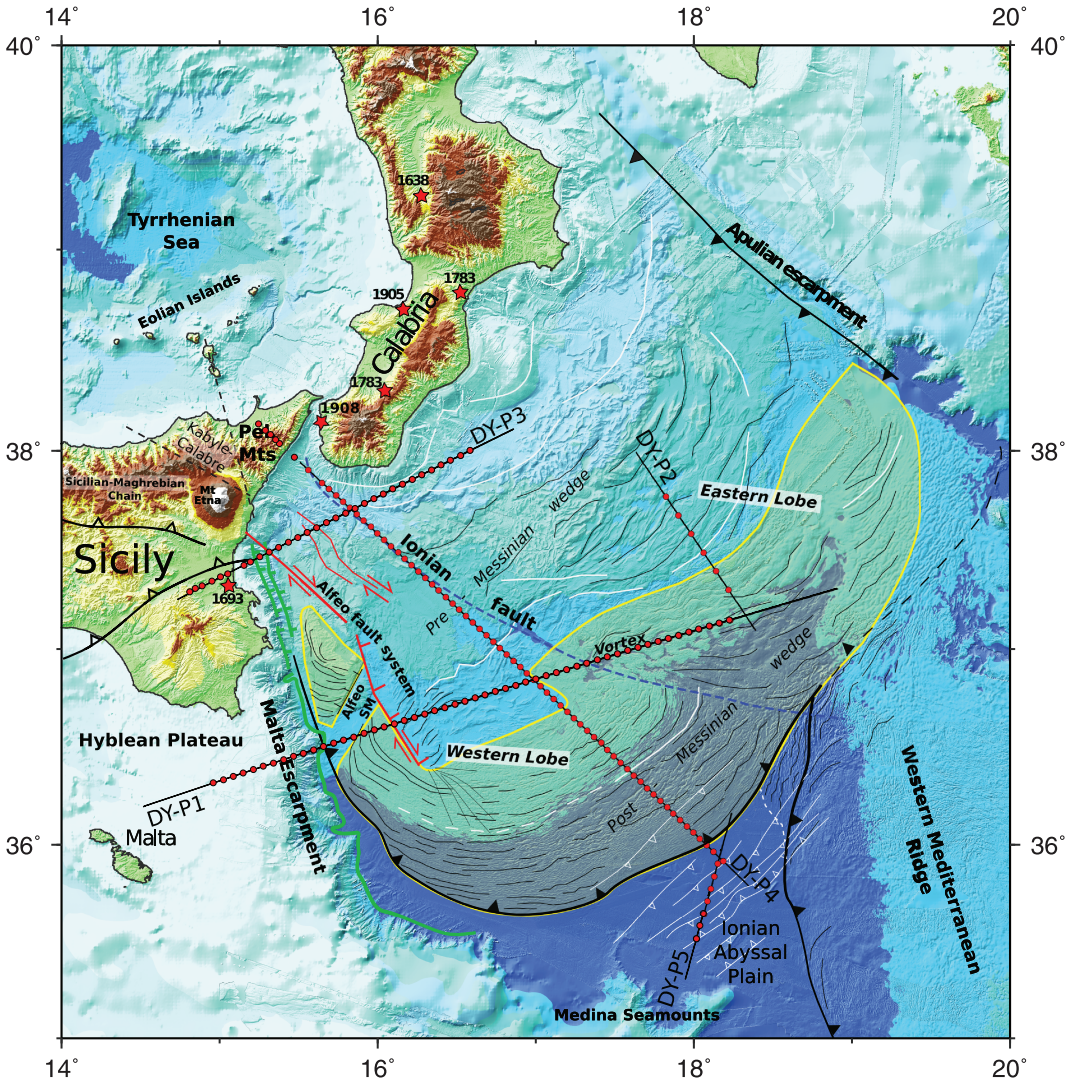

Figure 2. Tectonic map of the study area. Ocean-bottom seismometers and land stations are marked by red dots. Red stars mark hypocenters location of historical earthquakes. CROP-M3 MCS profile is coincident to DY-P4 (Figure 5; Polonia et al., 2011). Bathymetry from Gutscher et al. (2017) (after Dellong et al., 2018). Yellow-shaded area marks the supposed extension of tectonically thickened evaporites in the Calabrian accretionary wedge.

good agreement with an opening at the Late Triassic/Early Jurassic of the Ionian Basin (Frizon de Lamotte et al., 2011). Other studies propose ages ranging from early Late Triassic (220 Ma; Speranza et al., 2012) to Late Jurassic to Early Cretaceous (Catalano et al., 2001).

Travel-time tomography using local or teleseismic events has been able to image downgoing slabs in subduction zones to depth of several hundreds of kilometers (e.g., Spakman et al., 1993;Spakman & Wortel, 2004 ; Wortel & Spakman, 2000). One of the first studies of the Italian region showed large-scale lithospheric inhomogeneity in the deep structure of the Tyrrhenian Sea (Scarpa, 1982). Positive travel-time anomalies interpreted to be a NW dipping subducting slab beneath the Calabrian Arc were later imaged from teleseismic events (Amato et al., 1993). Results from 3-D teleseismic tomography focused on the study region reveal the downgoing slab as a fast structure extending 350 km laterally from northern Sicily to southern Campania and 400 km vertically (Cimini, 1999). A more refined mantle tomography imaged a 150-km-wide slab window beneath the southern Apennines, which probably opened after a slab tear occurred between the Apulian continental subduction and the Ionian oceanic slab (Chiarabba et al., 2008). These results were refined using a denser data set and led to the proposition that the subducting lithosphere remains attached along a 100-km-long segment at the central portion of the Calabrian Arc (Neri et al., 2012). Global

tomography models clearly image a horizontal anomaly in the transition zone at a depth of 500 km, which is interpreted to be a flat-lying part of the Calabrian slab (Spakman & Wortel, 2004; Wortel & Spakman, 2000). The existence of a proposed STEP fault (Govers & Wortel, 2005; Wortel et al., 2009) was confirmed by tomographic and gravity modeling, with a proposed location of the faults in the Tindari and Crotone Basin (Neri et al., 2012, Figure 1 for location). Recent geodetic work provided evidence for toroidal flow around the retreating slab edges of the Calabrian subduction system expressed by counterclockwise rotations at the northern and clockwise rotations at the southern edge of the slab corresponding to movements predicted by STEP faults (Palano et al., 2017). Recent tomographic studies imaged a trench-parallel slab break-off on both sides of the slab, which might be still propagating, narrowing the slab (Barreca et al., 2016, 2018; Scarfì et al., 2016, 2018). Horizontal tearing affecting both sides of the slab was proposed to result in a narrowing of the subduction system and enhanced subsidence along the still-intact segment of the slab (Scarfì et al., 2018). In central Calabria the depth of the slab has been determined by source-receiver function analysis during a tomographic experiment. The results show that the slab is steeply inclined and that a 4- to 6-km-thick layer of low-velocity sediments is imaged between the oceanic crust and the continental Calabrian backstop (Piana Agostinetti et al., 2009).

Gravity anomalies at subduction zones are generally characterized by strong signatures that are linked to topographic effects, material density, and temperature heterogeneities in the lithospheric mantle and the crust or even forces and stresses induced by plate dynamics (e.g., Krien & Fleitout, 2008; Levitt & Sandwell, 1995 and references therein). Gravity anomaly lineaments parallel to the arc-trench axis are often observed along subduction zones. For example, a negative free-air anomaly is usually observed at the trench and above the downgoing slab and is interpreted as a result of a topographic effect or of the presence of a light crustal material entrapped within the subduction complex (Forte et al., 1993; Marotta et al., 2006). It was suggested that great earthquakes occur predominantly in regions with a strongly negative trench-parallel gravity anomaly (Song & Simons, 2003). Earlier studies in the Ionian Sea have shown that Bouguer gravity anomalies are consistent with young subduction of an intermediate foreland lithosphere beneath two opposing subduction systems, the Apennine-Calabrian system to the SW and the Hellenic system to the northeast (Moretti & Royden, 1988).

Determining the position of the slab at shallow depth compared to earthquake tomographic studies and using seismic and gravimetry methods remain difficult because of the thick accretionary wedge and the Messinian evaporite layers introducing velocity inversions and density anomalies. This study aims to shed light on the deep structure of the Ionian subduction interface below the Calabro-Peloritan backstop with a higher resolution than the above-mentioned tomography and receiver function studies.

1.3. Objectives of the Study

Four wide-angle seismic profiles were acquired to provide a 3-D image of the E Sicily margin and the western portion of the Calabrian subduction zone (Figures 1 and 2). Two profiles orthogonal to the E Sicily margin cross the Malta Escarpment and the transition between the continental crust of the Hyblean Plateau and the Tethyan oceanic crust of the deep Ionian Basin (Dellong et al., 2018). One profile close to the Medina seamounts was shot to characterize the nature of the crust below the IAP (Dannowski et al., 2019). Our work presents the findings of the 380-km-long dip line, intersecting the three other profiles, and thus provides a comprehensive 3-D structural view of the analyzed sector. The dip line crosses from the undeformed domain of the IAP, across the external (evaporitic) Calabrian accretionary complex and the internal (clastic) accretionary wedge, and all the way to the Peloritan continental domain (NE corner of Sicily), composed of Hercynian metamorphic basement currently forming the backstop of the upper plate. The objective of this combined data set is to image the complex 3-D transition between the adjacent and the overlapping crustal domains, as well as the deep expression of the lateral slab tear (STEP) fault. Among the open questions that remained following the previously published work are (e.g., Dellong et al., 2018) what is the geometry (depth, thickness, dip) of the downgoing oceanic crust and its relative position to the overlying backstop and how does the thickness and nature of the accreted and/or underplated sediments vary downdip. We analyze the first wide-angle seismic data compilation that can address this set of questions.

Furthermore, regional 3-D gravity modeling was performed with the aim to test end-member models for the slab depth in the Calabrian-Messina strait region. Specifically, in wide-angle profile DY-P3, the top of the subducting oceanic crust was not imaged (Dellong et al., 2018). The authors proposed two hypotheses for

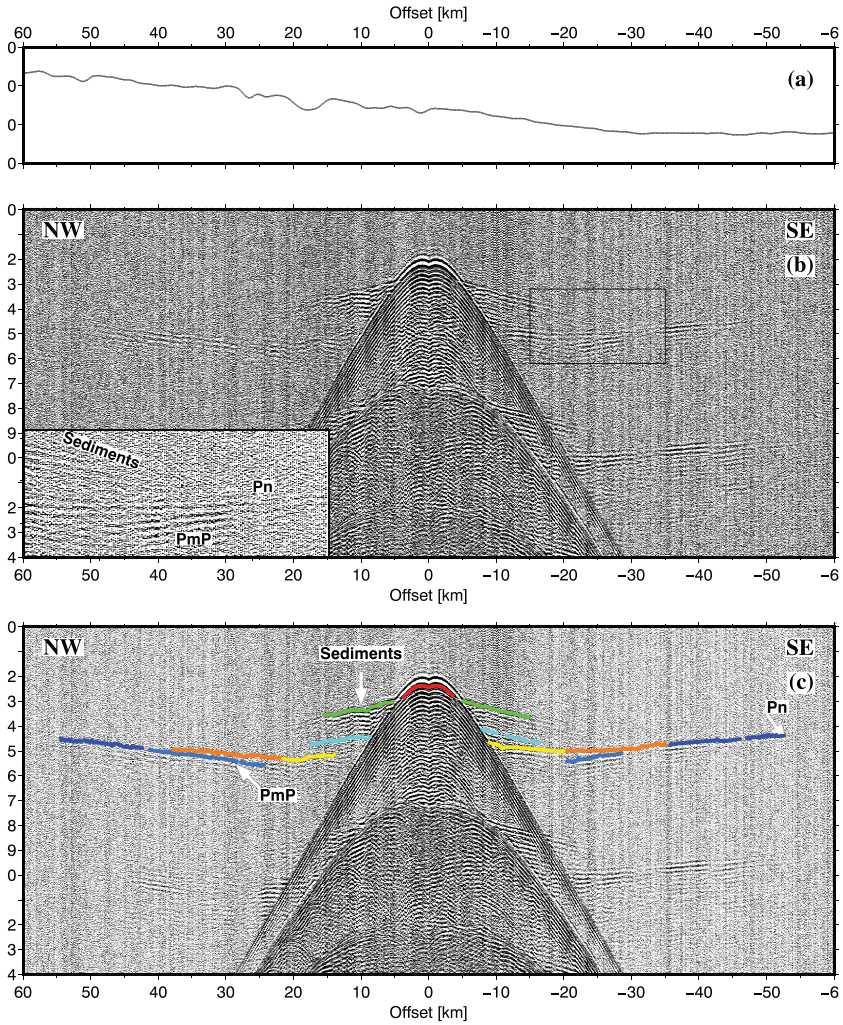

Figure 3. (a) Seafloor bathymetry along the sections shown below. (b) Data section from OBS 08 vertical geophone channel. The data are band pass filtered (3-4-24-36 Hz corner frequencies) and are reduced to a velocity of 6 km/s. (c) Data section OBS 08 with travel-time picks overlain.

its position (1) significantly below the Calabrian backstop and beyond the range of the seismic rays and (2) that the slab is part of the thick lower crustal layer of the backstop but not resolved by the OBS data given that velocity contrasts would be minor producing no high-amplitude reflection. As an intervening layer with mantle velocities (first hypothesis) will produce a strong, observable gravity anomaly, this problem can be resolved using 3-D gravity modeling.

2. Data Acquisition and Processing

The wide-angle seismic data were acquired in 2014 during the Dionysus survey, a collaboration between GEOMAR (Kiel, Germany), INGV (Rome, Italy), Ifremer, and the University of Brest (both Brest, France) onboard the R/V Meteor (M111 cruise). Additionally, we used gravity data from satellite free-air anomaly from the World Gravity Map (WGM2012—Bonvalot et al., 2012; Pavlis et al., 2012) for gravity modeling.

2.1. Wide-Angle Seismic Data

Three long and one shorter wide-angle seismic profiles were shot using an array of six GI-Guns of a total volume of 84 liters (5,440 $in.^3$) (Figure 2). This work focuses on the DY-P4 profile, which spans the Calabrian subduction zone along a SE-NW transect.

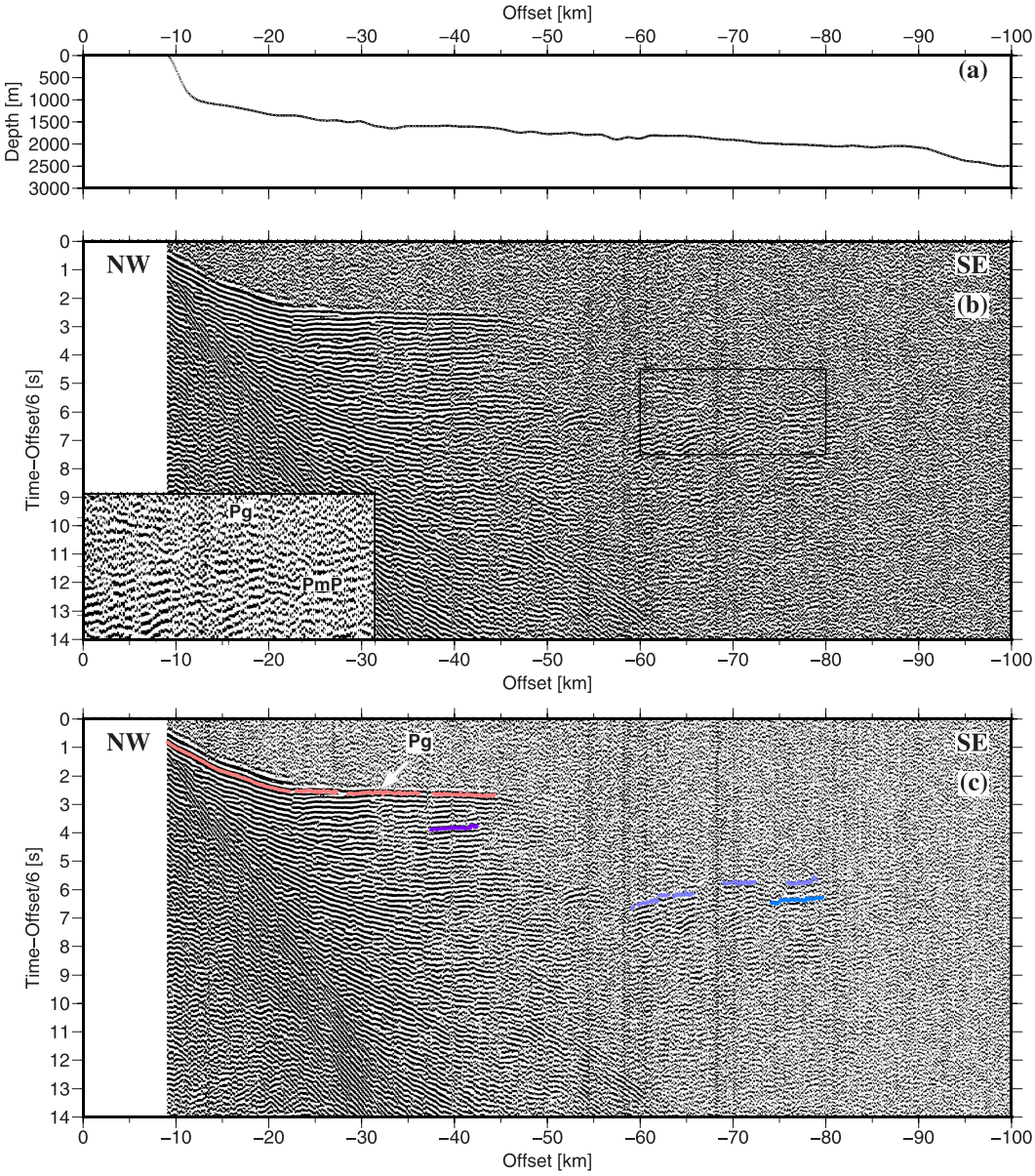

Figure 4. (a) Seafloor bathymetry along the sections shown below. (b) Data section from land-station S3 vertical geophone channel. The data are band pass filtered (3-4-24-36 Hz corner frequencies) and are reduced to a velocity of 6 km/s. (c) Data section from land-station S3 with travel-time picks overlain.

Half of the marine instruments used in this experiment were MicrOBS from Ifremer equipped with three-component 4.5-Hz geophones and a hydrophone both recording at a 4-ms sampling rate (Auffret et al., 2004). The other half consisted of ocean-bottom hydrophones from GEOMAR (Bialas & Flueh, 1999). Ocean-bottom seismometers (OBSs) were deployed on even position numbers and ocean-bottom hydrophones on odd position numbers. The land stations were six REF TEK 130S-01 equipped with short period velocimeter sensors with a 1-s dominant period. Their sampling rate was set at 8 ms. The seismic source used during the survey consisted of two subarrays of six GI-Guns. The 12 guns together provided a volume of 84 l (5,440 in^3) and were operated at 190 bar. The shooting interval was set to a constant 60 s for all profiles, resulting in a shot point interval of 150 m. The marine part of the profile is coincident with the deep reflection seismic profile CROP M2B, which was used in this study to constrain the geometry of the sedimentary layers (Polonia et al., 2011) (Figures 1 and 5).

We installed 61 ocean-bottom instruments along profile DY-P4 at 5- to 6-km intervals and 5 INGV land stations in Sicily along the prolongation of the profiles (see Figure 2). Data quality is good; however, arrivals are

Table 1
Name, Phase Number, and RMS Error for All Phases

Phase	Phase Number	Number of picks	RMS error [ms]
Water	1	3879	0.030
Sediment 1	2	1133	0.129
Sediment 2	3	3616	0.079
Sediment 3	9	823	0.190
Sediment 4	18	659	0.136
Sediment 5	16	306	0.162
Sediment reflection 1	4	676	0.107
Sediment reflection 2	5	326	0.086
Sediment refllection 3	10	102	0.193
Sediment reflection 4	19	1815	0.142
Top basement	6	1469	0.178
Oceanic lower crust	15	3494	0.139
Continental lower crust	11	3039	0.147
Intra-crustal reflection	12	506	0.229
PmP continental	7	422	0.203
PmP oceanic	14	811	0.189
Pn	8	895	0.086
All phases		23971	0.133

highly distorted, and energy is lost at long offsets probably due to the highly irregular sedimentary layer boundaries and the presence of salt leading to a velocity inversion in the sedimentary column (Figure 3 and Figure S1 in supporting information). The land-station data are of very good quality, and reflections picked from the data sections were one of the main inputs for the modeling of the subducting oceanic plate geometry (Figure 4). Initial processing was performed onboard, and profiles DY-P1 and DY-P3 were modeled using a forward approach (Dellong et al., 2018). This study uses an identical approach for profile DY-P4 to achieve intercomparable models. The OBS data were corrected for time and spatial drift during the deployment on board. First arrival time picking and a preliminary tomographic inversion were equally run on board; however, the resulting preliminary velocity models showed high uncertainties, due to the velocity inversion of the salt layer and the low density of seismic rays reaching lower crustal and upper mantle depth. Because of these difficulties, the data were modeled using the *Rayinvr* software (Zelt, 1999; Zelt & Smith, 1992) to be able to include additional information from coincident reflection seismic data and gravity modeling. This approach uses a combined forward and inversion approach to model layers of different velocities and velocity gradients. Layer depth and velocities are defined by the user in the first place. A smoothed inversion at velocity and depth nodes selected by the user can be used additionally to constrain the best-fitting solutions. Depending on the data quality, either the hydrophone or the vertical geophone data were used for the modeling.

Travel-time picking was performed when possible on unfiltered data sections. When necessary, a Butterworth frequency band-pass filter was used to enhance the signal/noise ratio. A total of 23,971 picks were used for the velocity modeling, including 17 phases (Table 1). The high number of phases is due to the lateral changes of the tectonic regime along this long profile. Although the absolute number of layers of the final velocity model is high (12 layers including water surface and Moho), the number of layers at any given position along the profile never exceeds 7. The high absolute number of layers can be explained by the lateral change of character of the sediments and crust from oceanic to the accretionary wedge and

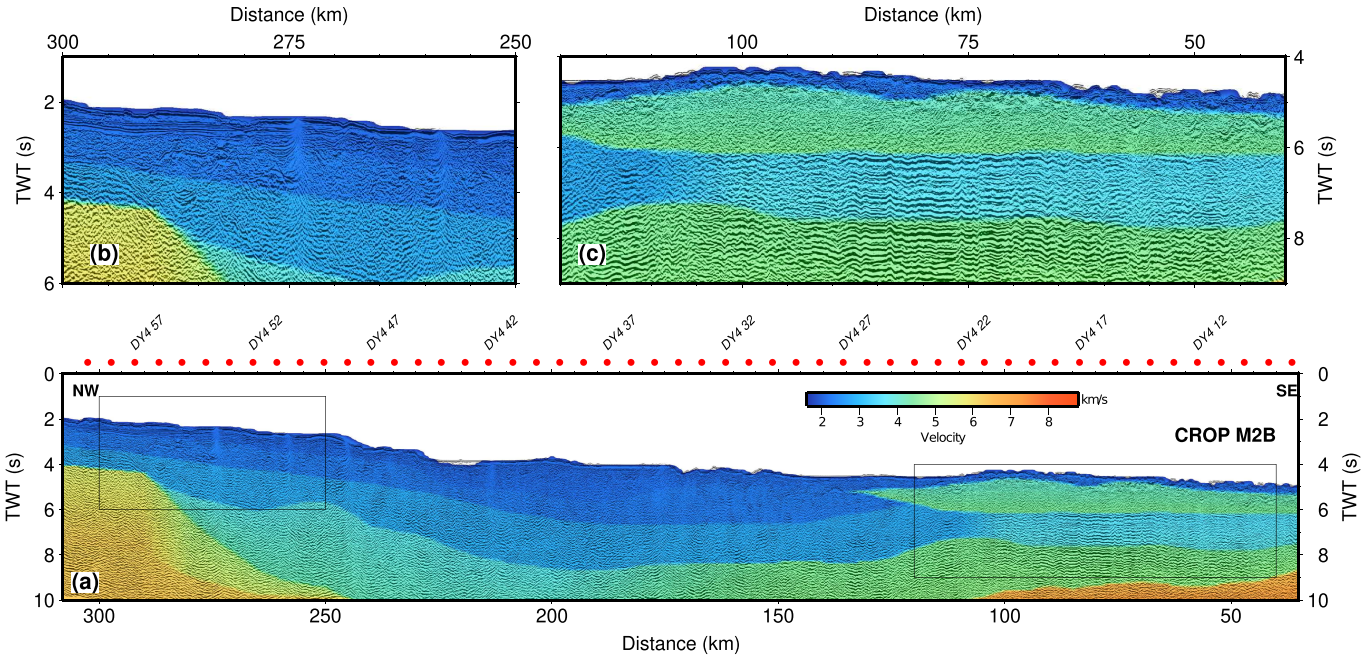

Figure 5. (a) Reflection seismic section of the coincident CROP M2B profile (Polonia et al., 2011) with velocities from our wide-angle seismic model underlain (see Figure 7). OBS locations are marked by red circles. (b) and (c) are zooms indicated on (a) to show more details of the reflection seismic data.

the Calabria block. Along the oceanic part of the profile, within the accretionary wedge, four sedimentary layers were modeled using reflected and turning arrivals. The second layer is characterized by a higher velocity than the underlying one, therefore inducing a velocity inversion. At the accretionary prism, four sedimentary layers were also picked. However, since the second and third layers show no lateral continuity to the oceanic region, two additional layers were defined to avoid confusing the readers and to demonstrate that the origin of those two layers differs from the ones to the SE. Similarly, two crustal layers were picked in the oceanic domain as well as in the backstop domain, resulting in four individual layers, which, however, are not continuous along the profile.

Key reflectors in the sedimentary layers were picked from the coincident CROP M2B time section (Figure 5 in this study and in more detail in Polonia et al., 2011) and were included in the wide-angle seismic model to better constrain the sedimentary layer geometry. The reflectors were converted to depth with the help of the OBS data. The model was extended on land to include the land-station data, but no reverse shots exist from the land part of the profile. The OBS data constrain sedimentary, crustal, and upper mantle parts of the model in the marine model. The land-station data provide constraints on the deep geometry of the necking zone. No turning wave arrivals from shallow layers on land exist as shots were only produced along the marine part of the profile (Figure 6).

2.2. Gravity Modeling

To evaluate the impact of different scenarios for the slab depth along the DY-P3 profile, three different models were constructed differing only in the depth of the slab. The first model is the (1) *reference model*, built to closely fit the predicted free-air anomaly from the model to the measured one. Then, two end-member models were built to test a (2) *shallow slab* hypothesis (5-km-shallower slab) and a (3) *deep slab* hypothesis (15 km deeper) (detailed explanations are given in Text S1).

3. Results

In the following section, the results from the velocity modeling are presented together with their error estimation. The results from the 3-D gravity models constructed in this study are presented thereafter.

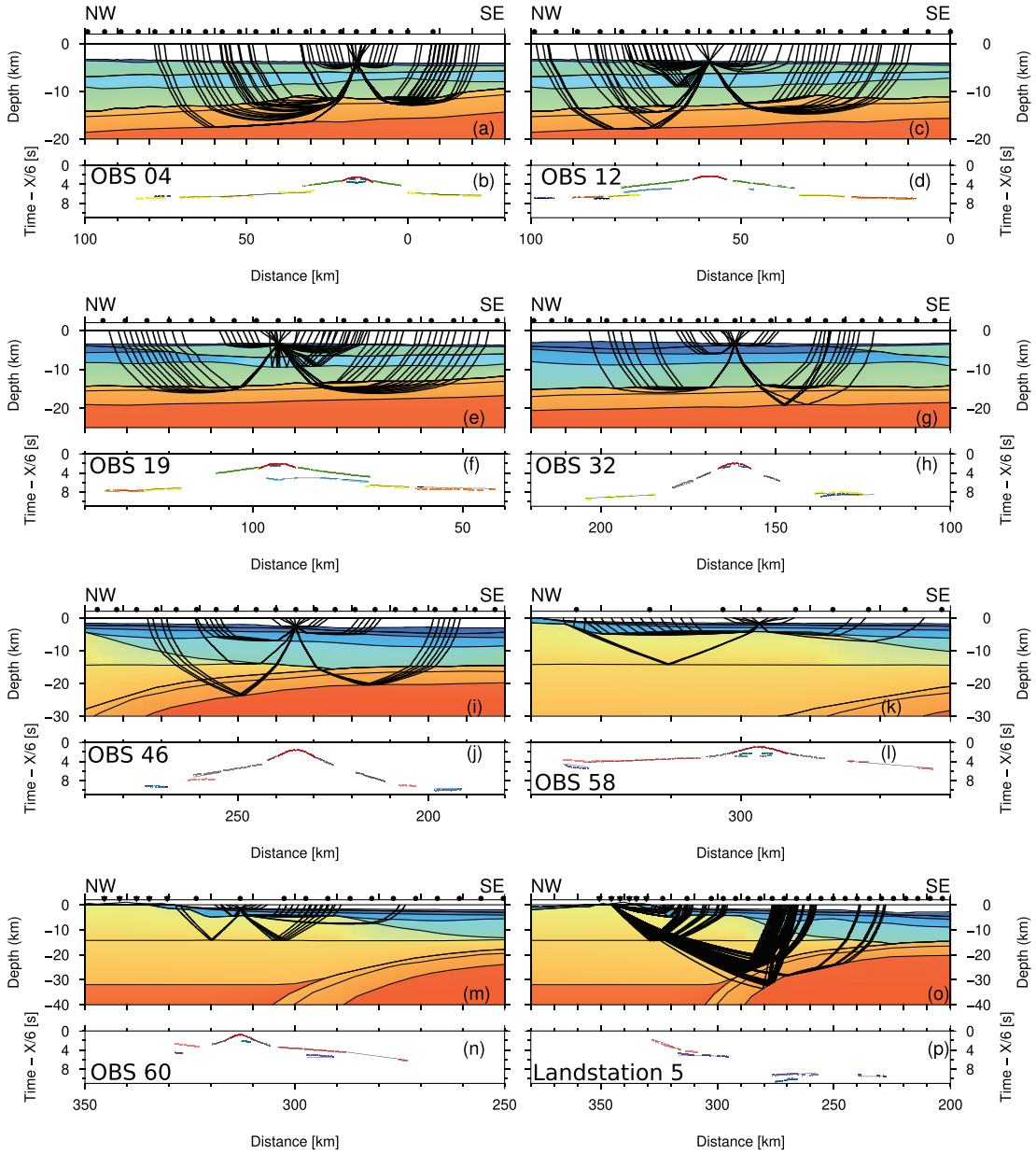

Figure 6. Panel a, c, e, g, i, k, m, and o model layers and raypaths of every 10th ray and panel b, d, f, h, j, l, n, and p corresponding travel-time picks and predicted arrivals (black lines). OBS positions are marked in the lower panels.

3.1. Seismic Velocity Model

The final velocity model is composed of five sedimentary units, an oceanic crustal layer subdivided into two layers (corresponding to Layers 2 and 3) and a Calabrian crustal block composed of two layers (Figure 7). The deepest layer corresponds to the lithospheric mantle; however, it's velocities are only constrained by diving rays in the oceanic part. The first sedimentary layer has a velocity between 2.0 and 2.3 km/s and a variable thickness between several hundreds of meters and 2–3 km. Along model distance 30 to 140 km, the second sedimentary layer is characterized by velocities between 4.5 and 4.8 km/s and with a thickness between 2 and 5 km, which is characteristic for the Messinian evaporite layer located in this part of the accretionary wedge. Toward the NW this layer thickens before being pinched out by the sedimentary units of the inner part of the accretionary wedge that has lower velocities between 2.3 and 2.35 km/s and a thickness of 2–3 km. The third sedimentary layer extends from the edge of the evaporite layer toward the NW with a variable thickness of ~3 km and velocities of 2.30–2.35 km/s. It was modeled as a separate layer as the velocities

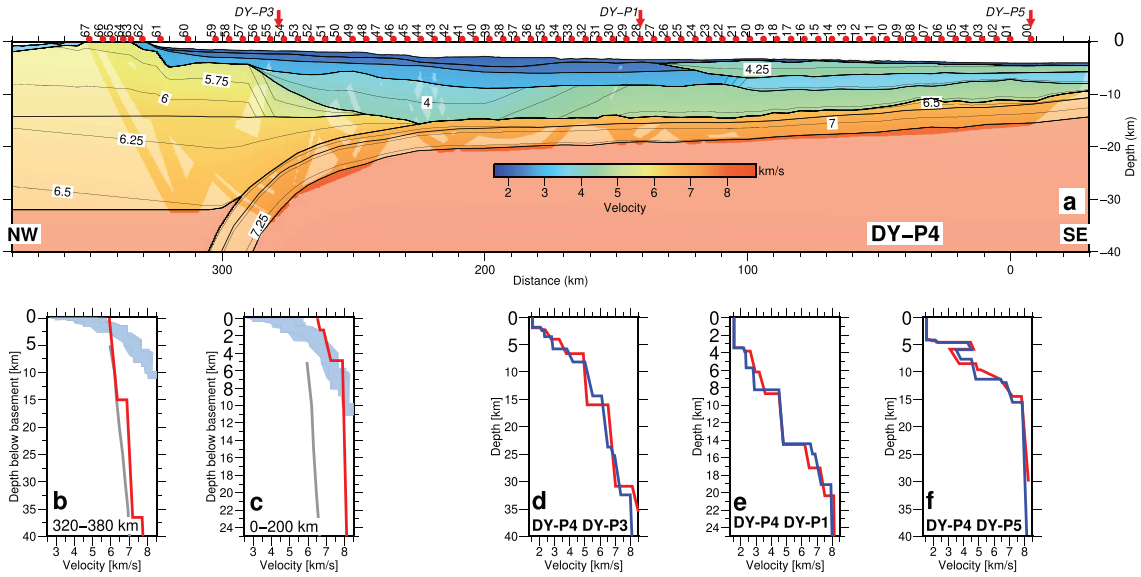

Figure 7. (a) Final velocity model of the profile DY-P4. The velocities are contoured every 0.25 km/s, and shaded areas are constrained by rays. Red dots mark the position of the seafloor instruments, and arrows mark the crossing points with DY-P1 and DY-P3 profiles. (b) and (c) Averaged velocity-depth profiles underneath the basement for the Ionian Basin and the Sicily crust. Blue envelope represents the velocity compilation for Atlantic oceanic crust from White et al. (1992) and gray thick line the velocity compilation for extended continental crust from Christensen and Mooney (1995). (d), (e), and (f) Velocity-depth profiles at the crossing. Red line is the DY-P4 profile, and blue lines trace the DY-P1 and DY-P3 profiles.

change abruptly from the evaporitic layer. The fourth sedimentary layer presents a lateral velocity change with higher velocities where it is underlying the evaporites of the outer accretionary wedge (3.50–3.80 km/s) than in the inner accretionary wedge (2.80–2.90 km/s). The lowermost sedimentary layer has a velocity between 4.5 to 4.8 km/s in the SE and 3.8 to 4.2 km/s in the NW. Together the thickness of the sedimentary cover varies between 5 km in the SW and 18 km at 230-km model distance. The Calabro-Peloritan block is covered by only 2–3 km of sediments. The oceanic crust is 5–6 km thick with velocities increasing from 6.5–7.2 km/s to 6.8–7.4 km/s toward the NW and has been subdivided into two distinct layers of ~2- and 4-km thickness. The Calabro-Peloritan block has a thickness of 30 km and was subdivided into two layers with velocities between 5.5 and 6.6 km/s diminishing to only 5.3 km/s at the tip of the backstop.

The MCS and the wide-angle seismic section show good agreement as the shallow sedimentary layers as the layer geometry was picked on the migrated time section (Polonia et al., 2011); however, MCS data offer a finer resolution of certain structures of the subduction system (i.e., thrust faults, slope basins, and inverted structures in the accretionary wedge) than deep-sounding wide-angle seismics (Polonia et al., 2011).

3.2. Error Calculations

The error between the picked arrival time and the predicted time from forward modeling indicates the fit of the model to the data. The number of picks and root-mean-square travel-time residual for all phases are listed in Table 1. Error calculations included the calculation of the node uncertainty smearing into neighboring parts of the model (spread point function) (Figure S2b), the resolution of the individual model nodes (Figure S2d), and the number of rays passing through the different layers (ray hit count) (Figure S2b). We also used “Vmontecarlo” software to produce a detailed analysis of the velocity uncertainties (Loureiro et al., 2016) (Figure S3). A detailed description and resulting figures are shown in Text S2 and Figures S2 and S3. Results from the error estimation show that the sedimentary and oceanic crustal domains are well constrained by reflected and turing rays. Here resolution is high with hit counts higher than 5,000 per cell, and smearing of uncertainties is low. Resolution is lower in the Calabrian lower crustal layer with only few rays passing through the layer and underneath the salt layer due to the velocity inversion from the salt to underlying sedimentary layers. The Monte Carlo inversion shows a good fit with uncertainties not exceeding 1.0 km/s for the deepest layers.

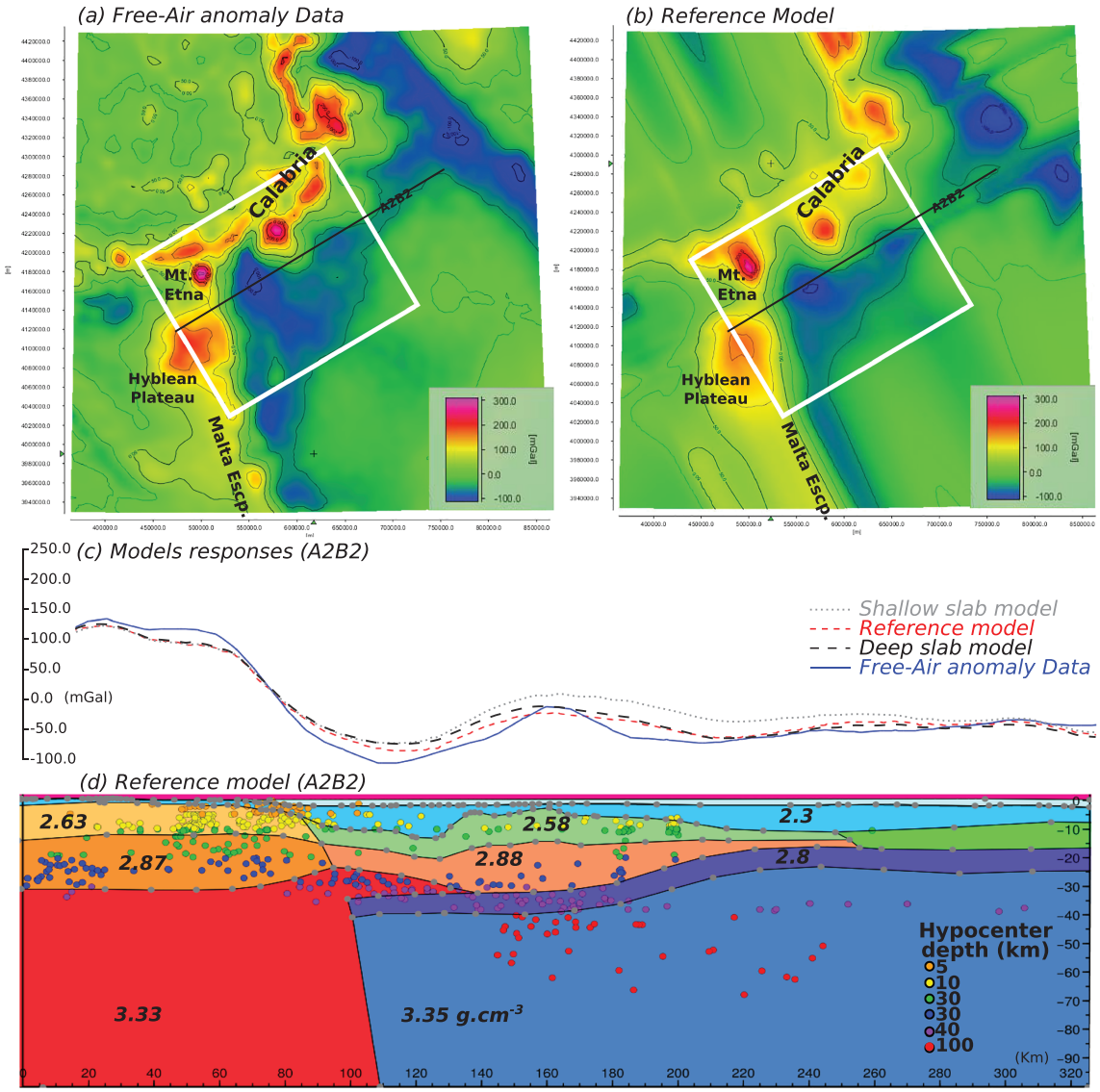

Figure 8. (a) Map of the free-air gravity anomaly (WGM2012—Bonvalot et al., 2012; Pavlis et al., 2012). (b) 3-D reference model gravity response. White rectangle shows the area of interest around the A2B2 profile (black line). (c) Gravity response of the different 3-D models (solely varying the oceanic slab depth) along the A2B2 profile. (d) A2B2 cross section extracted from the reference model, showing each individual layer and their densities. Earthquake hypocenters, projected from 10 km onto the profile, are shown by small circles colored by depth.

3.3. Gravity Models

In the Ionian Basin, the free-air anomaly is increasingly positive toward the S (Figure 8). The Apulian and Malta Escarpments are characterized by strong positive free-air anomalies. In central Sicily a negative anomaly contrasts with the positive free-air anomaly of Mount Etna, the Peloritan Mountains, and the Hyblean Plateau. In the Tyrrhenian Basin, a relatively homogeneous anomaly is observed with a value of approximately 50 mGal with the exception of the Eolian Islands presenting stronger anomalies.

The 3-D gravity models were built to reproduce these main features observed in the free-air anomaly. The long wavelength features of the free-air anomaly data are well reproduced throughout the three 3-D gravity models, showing that the deep density variations are explained by our models. Short wavelength variations are less well reproduced, meaning that some shallower features may be missing in the models.

The *reference model* places the top of the oceanic crust at a depth of about 30 km along this profile comparable to the wide-angle seismic model. For the *deep slab* model, the top of the oceanic crust is set at a depth of about 45 km along the A2B2 cross section. The slab then deepens to 60 km to the N-E along the GH cross

section allowing to observe the 3-D effect of a high-density body sandwiched in between the Calabrian continental crust and the oceanic crust. The calculated anomaly from this *deep slab* model increases by about 20 mGal with respect to the *reference model* and also affects the resulting anomaly beyond the direct slab depth deepening zone, in an area greater than 30 km. To the N, along the GH cross section, the slab deepening resulted in an increase of 10 mGal in the calculated anomaly in comparison to the reference model and in the S, along the ST cross section, in an increase of less than 5 mGal.

For the "shallow slab" model, the oceanic crustal layer depth was decreased to 20–25 km along the A2B2 cross section. This configuration is a more realistic hypothesis suggested in the past (Dellong et al., 2018). This model resulted also in an increase of the calculated gravity anomaly with respect to the reference model. But this increase is significantly greater than the one calculated for the "deep slab" model and is about 30 mGal. This modification does not affect the gravity anomaly at a large wavelength as this increase is only calculated for the areas that are close to the modification (less than 10 km along the cross section). To the N (along the GH cross section), we observed a small effect of this modification on the gravity anomaly (less than 5 mGal). However, it is characterized by a decrease of the anomaly in comparison to the reference model. In addition, to the S, along the ST cross section, this shallow slab model shows an increase of less than 5 mGal of the calculated gravity anomaly.

Three mantle densities were used to satisfactorily fit the data. These reflect three different geodynamical origins: a continental Hyblean mantle layer derived from the wide-angle velocity models (at 3.33 g/cm^3 shown in red in Figure 8 in more detail in Figure S4 and Table S1), an oceanic mantle layer (3.35 g/cm^3, in blue), and a back-arc mantle layer (3.22 g/cm^3, in pink). The relative difference of these values depends on the depth of the gravity model. However from preliminary tests, it is clear that models using one single density for the mantle do not allow to sufficiently fit the data. These last two layers were obtained by extrapolating the tomographic models (Scarfì et al., 2018) and therefore do not have a corresponding velocity in Table S1, which provides only velocities from wide-angle seismic modeling. The difference between the Hyblean and the Tethyan oceanic mantle domains is small and can be explained by several factors, such as mantle composition or thermal state. However, the density of the Tyrrhenian mantle is significantly different as also observed in the tomographic model (Scarfì et al., 2018). This difference is probably related to the post–Messinian back-arc extension, subduction-induced mantle convection, ensuing asthenospheric upwelling, and associated very high heat flow (Zito et al., 2003).

2-D gravity models produced using the "xgravmod" software of Colin Zelt along the profile DY04 are shown in the electronic supplements (Zelt, 1999; Text S3 and Figure S5). In these more detailed model densities from the seismic velocities, the sedimentary and oceanic crustal sections and the mantle velocities from the 3-D gravity modeling were taken into account. The resulting fit is high and allows to reproduce small gravity anomalies unresolved by the 3-D models.

4. Discussion

4.1. Gravity

The results obtained from the three 3-D gravity models show that the reference model has the best fit to the free-air gravity anomaly. In this reference model, the top oceanic crust is located at around 25- to 30-km depth along the A2B2 cross section (specifically along the DY-P3 velocity model). Based on the hypothesis that the recorded seismicity is predominantly intracrustal, the corresponding slab depth is in good agreement with either the reference model or the shallow slab model along the DYP3 profile. The three gravity models allow us to conclude that a mantle wedge is highly unlikely to exist below the Calabrian backstop along the DY-P3 velocity profile. The models show relatively large uncertainties concerning the depth of the interfaces of ±2.5 km for the Moho interface and the top of the oceanic crust. These results are in agreement with the DY-P4 velocity model and also the tomographic model from Scarfì et al. (2018). Three different lithospheric mantle densities enabled us to reproduce the large-scale regional observed free-air gravity anomaly and then to test the three slab depth hypotheses. These densities were attributed to the Tethyan oceanic domain (3.35 g/cm^3), the mantle below the Hyblean Plateau (3.33 g/cm^3), and the mantle of the Tyrrhenian back-arc domain (3.22 g/cm^3), respectively. The difference between the Hyblean and the Tethyan mantle domains is fairly small and can be explained by several factors, such as composition or thermal state of the mantle. However, the density of the Tyrrhenian mantle is significantly different as also observed in the

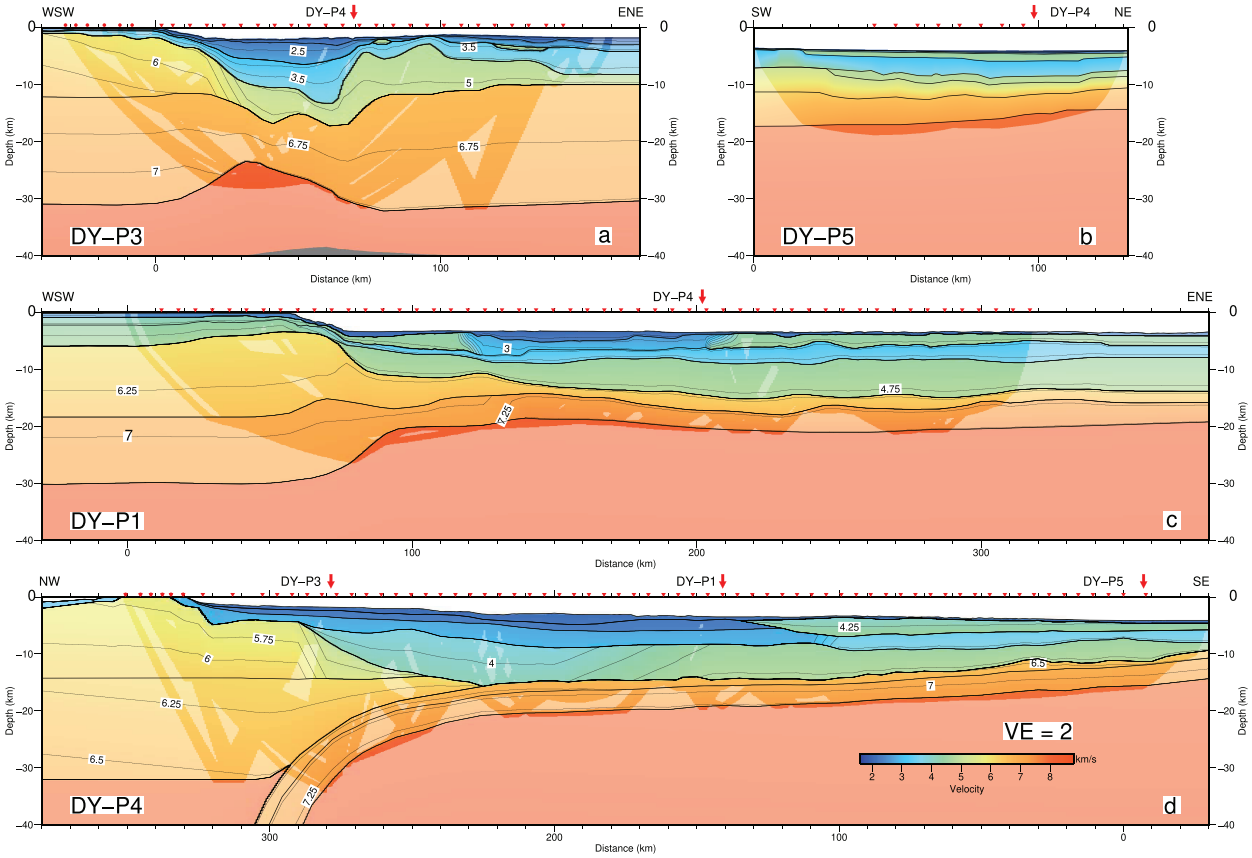

Figure 9. Final velocity models of the wide-angle seismic profiles DY-P3 (a), DY-P5 (b), DY-P1 (c), and DY-P4 (d). Crossings between profiles are marked by red arrows and OBS positions by inverted triangles. Vertical exaggeration is 2.

tomographic model (Scarfì et al., 2018). This difference is probably related to the post–Messinian back-arc extension, asthenospheric upwelling, and associated very high heat flow (Zito et al., 2003).

4.2. Velocity Models

A comparison of the DY-P4 velocity model with the three previously published velocity models (DY-P1, DY-P3, and DY-P5) (Dannowski et al., 2019; Dellong et al., 2018) provides a 3-D view of the Ionian Basin (Figure 9). The fit at the crossing points is good, with slight differences that may be due to anisotropy or data quality (Figures 7d–7f). Sedimentary thickness in the basin is highest at the backstop contact (10–12 km). The Messinian salt layer is imaged along profiles DY-P1, DY-P4, and DY-P5 with a thickness of up to 4 km. A layer of high-velocity sediments is imaged in the southern part of the basin (4.5–4.8 km/s). This high *P* wave velocity layer, showing parallel high-amplitude reflections, has long been described below as the IAP (de Voogd et al., 1992; Gallais et al., 2011; Makris et al., 1986; Minelli & Faccenna, 2010) and likely represents Jurassic deep-water carbonates, the only sedimentary rocks with such high velocities aside from halite (Anselmetti & Eberli, 1993). Oceanic crust underlying the basin is ~5 km thick, implying it is thinner than normal Atlantic Ocean crust from existing compilations throughout the basin, which has a mean thickness of 7.1 km (White et al., 1992). Crustal thickness increases abruptly at the Malta Escarpment (DY-P1) and at the Sicily margin (DY-P3) and at the Peloritan backstop (DY-P4), indicating the presence of continental crust in these domains (Figure 9). Similarly, in both DY-P3 and DY-P4 velocity models, the upper crustal velocities increase laterally toward the continental blocks of the Sicily margin (DY-P3, from 5.0 to 6.0 km/s) and Peloritan backstop (DY-P4, from 4.75 to 5.75 km/s). These two continental domains differ in their lower crustal layers with higher velocities in the Sicily margin. While the DY-P1 and DY-P3 are imaging the same continental Sicily margin through the Malta Escarpment, profile DY-P4 images a different continental block that is likely related to Peloritan backstop, inherited from the rollback of the Calabrian subduction. Another discrepancy between DY-P3 and DY-P4 is the presence of the slab (Figure 9 and Figure S6). While along DY-P3 no slab

was modeled, along the profile DY-P4, the slab is clearly imaged by the data from the land stations. This difference is due to the fact that the data quality of the land stations along DY-P4 is very high, and from OBS data alone on DY-P3, the slab could not be detected. Furthermore, the ENS-WSW orientation of profile DY-P3 very close to and parallel to the NW dipping slab hinge was unfavorable for recording deep crustal or upper mantle arrivals, as most of the seismic energy from the air gun shots would be transmitted downdip to the NW and off profile. The Moho depth along model distance 80–120 km on profile DY-P3 (31 km) corresponds to the depth of the oceanic Moho along DY-P4; however, the backstop-slab interface was not detected along DY-P3 (Figure 9). This result is in good agreement with results from the gravity modeling. In the S DY-P4 intersects with profile DY-P5 where both profiles image thin crust interpreted to be of oceanic origin (Dannowski et al., 2019).

Comparison of these results with existing compilations of crustal thickness and Moho depth shows a good agreement in the center of the basin (Nicolich et al., 2000), but significant differences exist at the Sicily margin and the Malta Escarpment, where the older studies propose relatively thin crust (~24 km) compared to our data that suggest a thickness of up to 30 km. These differences are probably due to the paucity earlier, wide-angle seismic data along these margins.

During the CAT/SCAN seismic experiment, 18 land stations were deployed to record teleseismic events during nearly 2 yr at the Sila Plateau in southern Italy. Using receiver functions from 586 events, the depth of the Ionian Moho was calculated to lie at around 35 km underneath the eastern part of Calabria gently dipping westward (Piana Agostinetti et al., 2009). The depth increases steeply to ~80 km beneath western Calabria. This study is located about 150 km N of DY-P4 so direct comparisons are not possible. However, the thickness of the Calabrian crust and steep dip of the subducting crust are in good agreement with our results. The authors also propose the existence of a 6- to 10-km-thick layer of underplated sediments between the Ionian and the Calabrian crust, which was not imaged in our velocity model. This might be due to the fact that our velocity model in the NW end is mainly constrained by reflected arrivals from the land stations, which might render the detection of low-velocity zones difficult. Also this observation is based on *S* wave velocities, which we were not able to model. Another explanation might be that our profile is located at the western edge of the subduction zone, where the crust is located at a shallower depth with respect to the center of the arc as imaged by tomography (Maesano et al., 2017; Scarfì et al., 2018). In central Calabria, the slab is highly arcuate and may transport a greater amount of sediments.

4.3. Results From Earthquake Tomography

A detailed tomographic image of the Calabrian subduction was constructed from local earthquakes (Scarfì et al., 2018) (Figure 10). The results indicate that the slab is continuous only below the southern Calabro-Peloritan arc where its curvature is highest. In the SW, deformation at the free slab edge has led to the detachment of a slab fragment and the formation of a slab window between 50 and 100 km (Scarfì et al., 2018). Comparing the wide-angle seismic velocity model, with results from the earthquake tomography and earthquake distribution, allows us to correlate the shallow layers to the deep mantle structures. The downgoing slab is continuous and steeply inclined in this region and can be traced as a high *P* wave velocity anomaly as well as by using the distribution of earthquake hypocenters. The Moho depths are similar in the Ionian Basin and in the part of the arc constrained by seismic rays. The thickness of the low-velocity accretionary wedge is similar as well. The tomographic model shows that the physical properties of the mantle differ between the Ionian and the Tyrrhenian Basins, which led us to use different values for our gravity modeling. The low-velocity anomaly in *S* wave velocity indicated from receiver function analysis (Piana Agostinetti et al., 2009) does not correspond to a low-velocity zone in *P* wave velocity in the tomographic model.

Particularly interesting feature of the Calabrian slab geometry as constrained by our wide-angle seismic data and the tomographic image is the extremely shallow average dip of 1.3° of the subducting oceanic crust over the frontal 200 km (deepening from 11 km to about 16 km), the slab hinge where the slab dip increases abruptly from 2–5° to 60–70° over a distance of ≤50 km. By comparison with regional tomography data, only the very steep dip of the deep slab below 60-km depth (about 70°) can be deduced. One of the novelties of this work is the first successful imaging using wide-angle seismic data of a slab hinge with such an extremely abrupt steepening.

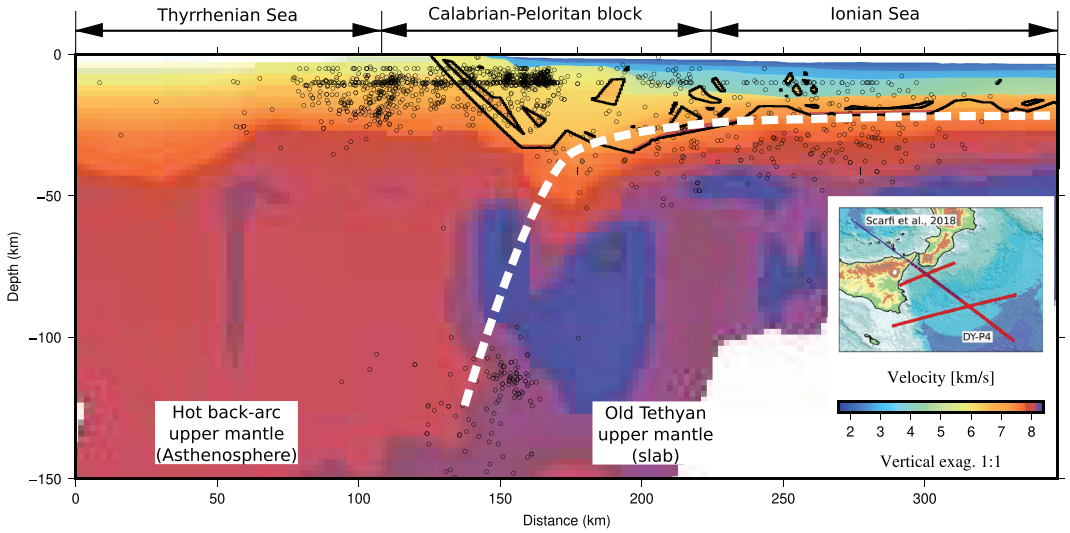

Figure 10. Profile extracted from the tomographic model of Scarfì et al. (2018) with layer boundaries from the DY-P4 profile overlain. Earthquakes projected from a maximum of 5-km distance along the profile are marked as black dots. *P* wave velocities in the model are indicated by the scale at right (in the inset). Inset: Bathymetry of the study region (Gutscher et al., 2017). Blue line shows position of the tomography model and red dots OBS positions.

Finally, the very narrow geometry of the Calabrian slab (lateral width ≤ 200 km) (Neri et al., 2012; Scarfì et al., 2018) may contribute to the steep dip. Indeed, numerous analog (Funiciello et al., 2006; Schellart, 2004) and numerical modeling studies (Govers & Wortel, 2005) have shown that for narrow slabs, the toroidal flow around the slab is facilitated, enabling the slab to roll back more rapidly and contributing to increasing its dip (see also section 4.4 below on deep slab geometries). SKS splitting observed in the mantle below southern Italy confirms strong toroidal flow behind the Calabrian slab (Civello & Margheriti, 2004). Such extremely narrow slabs (e.g., Calabria, Gibraltar) were excluded in the global analysis of subduction zones since their segment lengths were considered too short to be representative of typical slab behavior free of edge effects (Heuret & Lallemand, 2005; Lallemand et al., 2005).

4.4. Narrow Curved Subduction Zones and Deep Slab Structure

Global travel-time tomographic images of the upper mantle reveal slab geometries at large scale (Bijwaard et al., 1998) and can also image ongoing geodynamic processes such as slab tearing and slab detachment (Wortel & Spakman, 2000). Here we present three examples of deep slab geometries, two from narrow curved arcs (Gibraltar and Calabria) and one from a much longer laterally continuous subduction zone (Northern Honshu), unsegmented over nearly 1,000 km (Figure 11). The Calabrian subduction and Gibraltar subduction are possibly the narrowest arcs in the world, with lateral widths of ≤300 km and ≤200 km, respectively (Faccenna et al., 2004; Gutscher et al., 2002; Gutscher et al., 2017; Wortel & Spakman, 2000). In both cases wide-angle seismic studies have concluded that the downgoing lithosphere is most likely oceanic in nature and of Jurassic age (Sallarès et al., 2011; Dellong et al., 2018). Both subduction systems are characterized by extremely wide (~200 km downdip direction) accretionary wedge complexes, with very shallow surface angles and thus narrow tapers (Dellong et al., 2018; Gallais et al., 2012; Gutscher et al., 2002, 2009, 2012; Gutscher et al., 2017). There is a broad consensus that apart from their large-scale morphotectonic similarities, both subductions formed through rollback of narrow slabs over the past 5–10 million yr (Chertova et al., 2014; Faccenna et al., 2004; Gutscher et al., 2002; Gutscher et al., 2017; Palano et al., 2017; van Hinsbergen et al., 2014). The overall slab geometry of both systems is also largely similar. As discussed above, the dip of the downgoing plate is very shallow below the accretionary wedge (typically 1–5°). The plate dip increases abruptly below the overriding continental fore-arc block to 30–45° where the slab reaches depths of 50–100 km (Figures 11a and 11b). Below 100-km (for Calabria) and below 150-km depth (for Gibraltar), the slab dip increases to >60°, locally approaching a subvertical geometry (Figures 11a and 11b). There are also deeper subhorizontal high *P* wave velocity anomalies between 600- and 660-km depth, below the Betics (S Spain) and below Corsica-Sardinia, related to the older portions

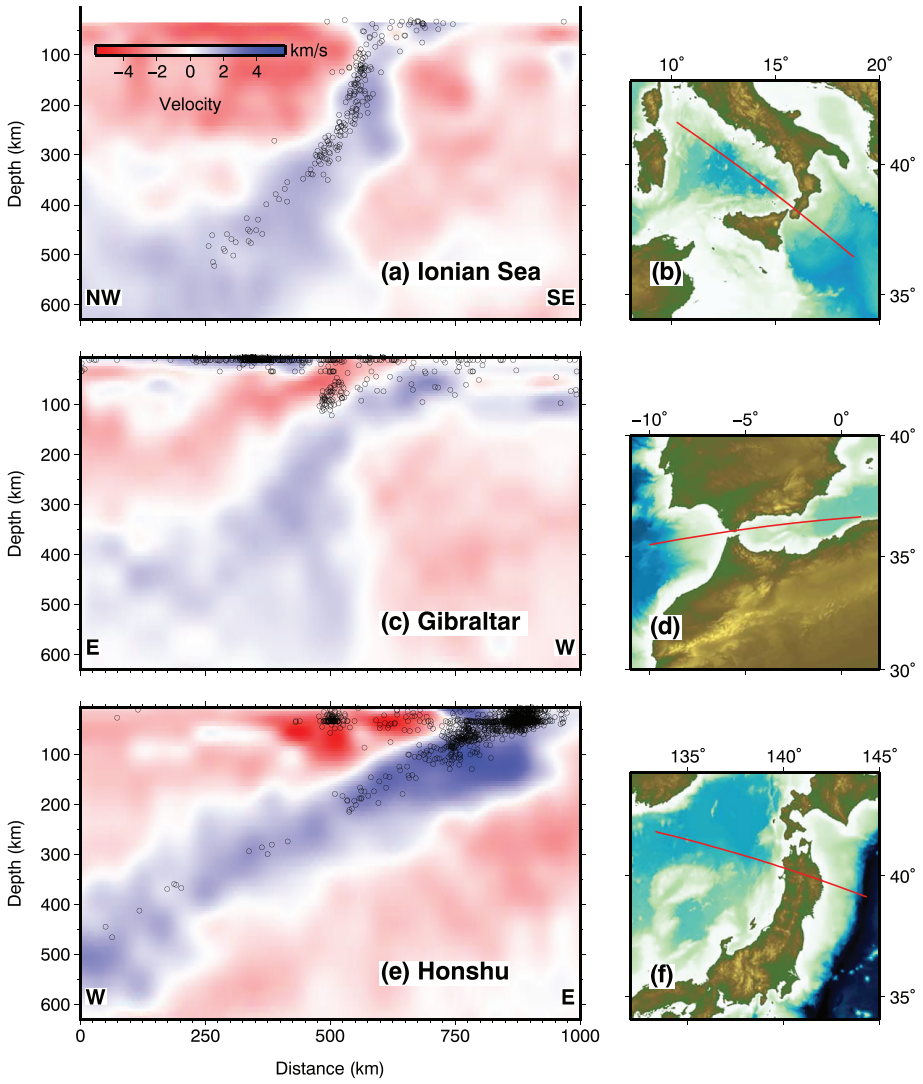

Figure 11. (a) Cross section in the global earthquake travel-time tomographic model UU-P07 (Amaru, 2007) through the Ionian Sea subduction zone. (b) Location map for the profile in panel (a). (c) Cross section in the UU-P07 tomographic model (Amaru, 2007) through the Gibraltar subduction zone. (d) Location map for the profile in panel (c). (e) Cross section in the UU-P07 (Amaru, 2007) through the Honshu subduction zone. (f) Location map for the profile in panel (e).

of the Gibraltar and Calabrian subductions, respectively, which are already discussed at length by previous authors (Bezada et al., 2013; Chertova et al., 2014; Faccenna et al., 2004; van Hinsbergen, Vissers, & Spakman, 2014; Wortel & Spakman, 2000) and which are consistent with the long-term slab rollback kinematics, which have resulted in these narrow arcs. More recent detailed tomographic work using earthquake travel-time data from local seismic networks has imaged the lateral slab tears and nearby portions of detached slabs and concludes that these two systems are approaching the terminal stages of subduction (Bezada et al., 2013; Neri et al., 2009; Scarfì et al., 2018).

There are some differences between the tomographic images from the respective back-arc domains, however. The Calabrian backarc (below the Tyrrhenian Sea) shows a broader stronger low *P* wave velocity anomaly, than the corresponding back-arc domain from the Gibraltar subduction (below the Alboran Sea), which exhibits a thinner zone of higher-temperature asthenosphere at shallower depths (50–150 km), and further in the backarc presents a less pronounced and more heterogeneous anomaly (Figures 11c and 11d). While the estimated modern-day subduction velocities are very small for both subduction systems, 3–5 mm/yr for Calabria (Palano et al., 2012, 2017) and ~5 mm/yr for Gibraltar (Koulali et al., 2011; Palano et al., 2015), it is thought that the Tyrrhenian Sea back-arc basin had two major phases of opening linked to rapid

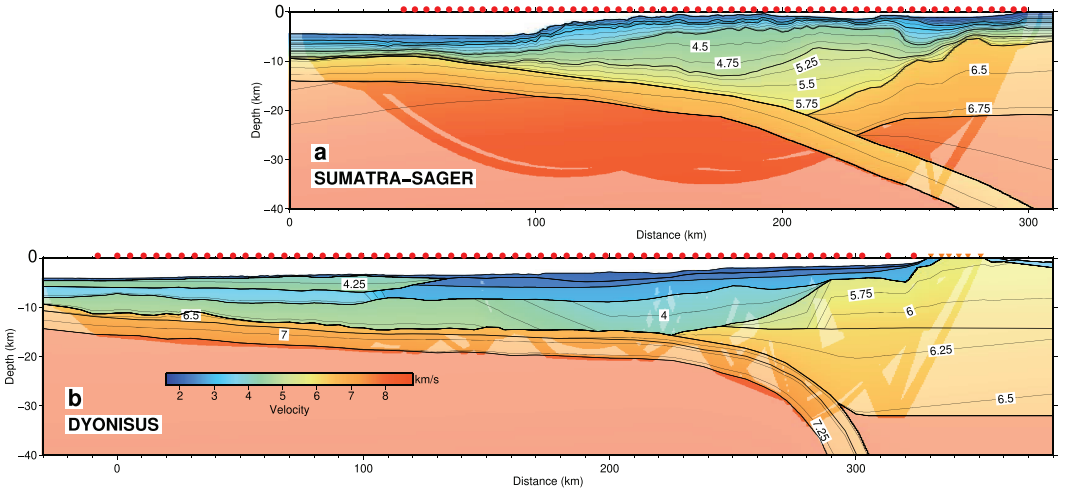

Figure 12. Comparison of the wide-angle seismic profiles from the (a) Sumatra SAGER cruise (Klingelhoefer et al., 2010) showing gradual flexure and a marked bulge expressed as a basement high around 40-km profile distance and (b) Dionysus DY-P4 showing a nearly constant extremely shallow plate dip (1–2°) and then a slab hinge between 250- and 300-km profile distance where the slab dip increases abruptly to >45°.

slab rollback, inducing vigorous mantle convection (Faccenna et al., 2001). Furthermore, the larger Tyrrhenian Sea back-arc basin evolved all the way to seafloor spreading (Marani & Trua, 2002), whereas the W Alboran basin, while highly extended, never reached seafloor spreading (Booth-Rea et al., 2007; Medaouri et al., 2014; Watts et al., 1993). A broader subducting segment (300 vs. 200 km) and a larger, fully developed back-arc basin both imply more vigorous convection in the asthenospheric wedge above the subducting Calabrian slab (Figures 11a and 11b).

The N Honshu subduction (NE Japan Trench) has a very different overall slab geometry with a nearly constant shallow (50- to 150-km depth) and deeper (200- to 500-km depth) slab dip of about 30–35° (Figures 11e and 11f). The age of the subducting lithosphere is Mesozoic, about 130 Ma (Mueller et al., 1997), and therefore rather similar to the estimated age of the lithosphere subducting below Calabria or Gibraltar. It should be noted, however, that in fact there is no statistically significant correlation between the age of the subducting lithosphere and the slab dip based on a global analysis of subduction zone parameters (Lallemand et al., 2005). Other factors play a more dominant role like the nature of the upper plate (continental vs. oceanic) or the overall kinematics of the forearc and the backarc (extension vs. convergence) (Lallemand et al., 2005). The reasons for the constant and very modest slab dip below N Japan and extending below NE China are probably related to an anchoring of the Pacific slab at the 660 discontinuity below NE China and a stationary trench (in a Eurasia-fixed reference frame) and to the large lateral width (1000 km) of the unsegmented Pacific slab, before changing its orientation at the Kurile trench. A long, laterally continuous slab favors poloidal flow, while limiting toroidal flow around the lateral slab edge, and creates a very stable kinematic configuration for the large-scale slab (Lallemand et al., 2005; Schellart, 2004). Finally, there are also major differences in the overall level of seismicity in the three slabs (Figures 11e and 11f). While the N Honshu slab is marked by abundant seismicity down to 200 km and then by scattered seismicity down to 500 km (Figure 11c), the Calabrian slab is also marked by abundant intermediate depth seismicity down to 300 km and thereafter by less abundant but still clearly marked seismicity down to 500 km (Figure 11a). In contrast, the Gibraltar slab exhibits a cluster of intermediate depth seismicity between 60- and 120-km depth and no deeper seismicity below (Buforn et al., 2004) (Figure 11b). It has been suggested that this is evidence for a horizontal tear (slab detachment) occurring here (Heit et al., 2017), though an alternative explanation is the presence of extreme bending stresses as the slab abruptly steepens (Gutscher et al., 2002). Deep-focus earthquakes occur below Granada (S Spain) (Buforn et al., 2011) and confirm the presence of a deep slab here interacting with the 660-km discontinuity (Bezada et al., 2013).

4.5. Comparison of Two Thick Accretionary Wedges With Thick Incoming Sedimentary Sections

If we compare the accretionary wedges from Sumatra and Calabria (Figure 12), the cross-sectional areas of the two accretionary wedges are quite similar. For Calabria the wedge is about 250 km wide (downdip width)

with a maximum thickness of 12–13 km and an incoming sedimentary thickness of 5–6 km. For Sumatra, the incoming sedimentary thickness is identical (5 km), and the width of 150 km and maximum thickness of 20 km are 40% less and 50% more than for Calabria, respectively. The main differences are the surface slope angles, which are much lower for Calabria (~1°) than for Sumatra (2–3° with an overall convex shape) and the dip of the downgoing plate. For Calabria as discussed above, it is a regular, constant 1.3° dip over 200 km, and then the dip steepens sharply (Figure 12). For Sumatra the dip is about 3° below the deformation front, and it increases progressively to 10° at 20-km depth (contact with the upperplate backstop at profile km 200). The dip remains roughly 10° down to 40-km depth (Figure 12A). The overall geometry of the Sumatra subduction resembles an ideally bulged lithosphere, with a marked 1-km-high flexural bulge visible in the wide-angle seismic data (Figure 12A, model km 50) but buried beneath the thick Bengal Fan sediments. There would be a deep-sea trench, characteristic of most subduction zones, were it not for the enormous quantity of sediments (5 km) drowning this morphological feature. The Calabrian subduction does not show this broad-scale flexure and has no flexural bulge. This may be in part due to the fact that it is a very narrow slab and that our seismic profile is sampling the edge of the subduction zone or due to the stiffness of the plate. In the SE and central part of the profile (Figures 11 and 12, model km 0–200), the oceanic crust is still attached to the W to the continental crust of the Hyblean domain. The slab dip increases abruptly NW of the termination of the lateral slab tear fault (model km 280–300).

A second observation from this comparison is that the accretionary wedge in the Ionian Basin is characterized by a very shallow slope in comparison to other subduction zones with thick accretionary wedges. This fact is possibly related to the presence of Messinian evaporites in a large part of the wedge, which will facilitate sediment sliding gradually down the slopes (Minelli & Faccenna, 2010) and therefore will facilitate the buildup of a large accretionary prism. The very low taper angle of the external Calabrian Arc accretionary wedge is comparable to that proposed for the neighboring salt-bearing Mediterranean Ridge by Kastens (1991) through analysis of sediment facies within the wedge. Low slope angles might be explained by the mechanical strength of the evaporites over a very weak basal detachment that favors outward growth rather than vertical stacking of accreted units (Polonia et al., 2011). The composition of sediments along the subducting plate and in the accretionary prism has a direct influence on the hydrogeology, fluid budgets, and geotechnical properties of the plate boundary (Underwood, 2007). Sediment thickness and the lithostratigraphy of the incoming plate influence the physical properties of the margin inducing lateral heterogeneities in the prism formation (Ike et al., 2008). Also, salt layers influence the tectonic deformation style and spatial variation in pore water salinity resulting in differences in fluid density and can therefore drive large-scale fluid and heat transport (Sarkar et al., 1995) impacting on the position of the updip limit of the seismogenic zone.

5. Conclusions

From gravity modeling we conclude that along the DY-P3 profile, the gravity model with the oceanic slab at an intermediate depth of about 25 km shows the best fit. This model implies that there is no mantle layer between the Calabrian backstop crust and the dipping slab. In order to obtain a good fit to the observed gravity anomaly and with respect to the tomographic models, the mantle densities in the Tethyan oceanic domain (3.35 g/cm^3) must differ substantially from those in the Tyrrhenian back-arc domain (3.22 g/cm^3). This is in good agreement with the fact that the basins are of different ages and with the presence of hot, convecting mantle/asthenosphere beneath the back-arc domain.

The velocity model for the DY-P4 profile images thin oceanic crust throughout the basin beneath the accretionary prism. At the NW end of the profile, the Calabrian backstop extends underneath the accretionary wedge to about 100 km SE of the Calabrian coasts. The thick accretionary wedge is divided into four layers comprising a high-velocity evaporitic layer and a high-velocity stratified layer deposited directly on top of the oceanic basement and probably consisting of deep-water carbonates. The presence of Messinian evaporites in a large part of the wedge causing a very low basal friction facilitates lateral spreading during convergence and favors construction of a very long, shallowly tapered accretionary prism.

Prolongation of the model using earthquake hypocenters and regional tomographic data indicates that the slab dip increases abruptly from 2–3° to 60–70° over a distance of ≤50 km underneath the Calabrian

backstop. This might be related to the rollback geodynamic evolution of the narrow Calabrian slab, which is similar to the Gibraltar slab showing a very comparable geometry.

Acknowledgments
We thank the captain and the crew of the R/V Meteor for the data acquisition during the marine survey. The *Dionysus* cruise (M111) was funded through the Deutsche Forschungsgemeinschaft (DFG). We also acknowledge Région Bretagne and Ifremer for funding the PhD scholarship associated to this work, as well as the University of Western Brittany and the LabexMer for their help and funding of this work. We would like to acknowledge the scientists and technical teams of the INGV for deploying the land stations and Bruno Marsset from Ifremer for the help in processing these data. Most of the figures from this paper were generated using the Generic Mapping Tools (http://gmt.soest.hawaii.edu), and the Seismic Unix software was used for processing the wide-angle seismic data (https://github.com/JohnWStockwellJr/SeisUnix/wiki) (Cohen & Stockwell, 2000). The free OpendTect from dGB Earth Sciences (https://www.dgbes.com/index.php/download) and the open source Qgis software (https://www.qgis.org/fr/site/forusers/download.html) were used for data processing and drafting of several figures. Upon request at http://doi.org/10.17882/52435, the ocean-bottom seismometer data used in this publication are accessible in standard SEGY format.

References

Amaru, M. L. (2007). *Global travel time tomography with 3-D reference models* (Vol. 274). Utrecht, Netherlands: Utrecht University.
Amato, A., Alessandrini, B., Cimini, G., Frepoli, A., & Selvaggi, G. (1993). Active and remnant subducted slabs beneath Italy: Evidence from seismic tomography and seismicity. *Annals of Geophysics*, *36*(2).
Anselmetti, F. S., & Eberli, G. B. (1993). Controls on sonic velocity in carbonates. *Pure and Applied Geophysics*, *141*, 287–323.
Argnani, A., & Bonazzi, C. (2005). Malta Escarpment fault zone offshore eastern Sicily: Plio-Quaternary tectonic evolution based on new multi-channel seismic data. *Tectonics*, *24*, TC4009. https://doi.org/10.1029/2004TC001656
Auffret, Y., Pelleau, P., Klingelhoefer, F., Geli, L., Crozon, J., Lin, J. Y., & Sibuet, J. C. (2004). MicrOBS: A new generation of ocean bottom seismometer. *First Break*, *22*(7), 41–47.
Barreca, G., Branca, S., & Monaco, C. (2018). Three-Dimensional Modeling of Mount Etna volcano: Volume Assessment, Trend of Eruption Rates, and Geodynamic Significance. *Tectonics*, *37*, 842–857. https://doi.org/10.1002/2017TC004851
Barreca, G., Scarfì, L., Cannavo, F., Koulakov, I., & Monaco, C. (2016). New structural and seismological evidence and interpretation of a lithospheric-scale shear zone at the southern edge of the Ionian subduction system (central-eastern Sicily, Italy). *Tectonics*, *35*, 1489–1505. https://doi.org/10.1002/2015TC004057
Bezada, M. J., Humphreys, E. D., Toomey, D. R., Harnafi, M., Davila, J. M., & Gallart, J. (2013). Evidence for slab rollback in westernmost Mediterranean from improved upper mantle imaging, Spain. *Earth and Planetary Science Letters*, *368*, 51–60. https://doi.org/10.1016/j.epsl.2013.02.024
Bialas, J., & Flueh, E. R. (1999). Ocean bottom seismometers. *Sea Technology*, *40*(4), 41–46.
Bijwaard, H., Spakman, W., & Engdahl, E. R. (1998). Closing the gap between regional and global travel time tomography. *Journal of Geophysical Research*, *103*, 30,055–30,078.
Bonvalot, S., Balmino, G., Briais, A., Kuhn, M., Peyrefitte, A., Vales, N., ... & Reinquin, F. (2012). World gravity map. Bureau Gravimetrique International (BGI), Map, CGMW-BGI-CNES728, IRD, Paris.
Booth-Rea, G., Ranero, C. R., Martínez-Martínez, J. M., & Grevemeyer, I. (2007). Crustal types and tertiary tectonic evolution of the Alboran Sea, western Mediterranean. *Geochemistry, Geophysics, Geosystems*, *8*, Q10005. https://doi.org/10.1029/2007GC001639
Bouillin, J. P., Durand-Delga, M., & Olivier, P. (1986). *Betic-Rifian and Tyrrhenian arcs: Distinctive features, genesis and development stages. In Developments in Geotectonics* (Vol. 21, pp. 281–304). Amsterdam, Netherlands: Elsevier.
Buforn, E., Bezzeghoud, M., Udías, A., & Pro, C. (2004). Seismic sources of the Iberia-African plate boundary. *Pure and Applied Geophysics*, *161*, 623–646.
Buforn, E., Pro, C., Cesca, S., Udías, A., & del Fresno, C. (2011). The 2010 Granada, Spain, deep earthquake. *Bulletin of the Seismological Society of America*, *101*(5), 2418–2430. https://doi.org/10.1785/0120110022
Byrne, D. E., Davis, D. M., & Sykes, L. R. (1988). Loci and maximum size of thrust earthquakes and the mechanics of the shallow region of subduction zones. *Tectonics*, *7*(4), 833–857.
Carminati, E., Negredo, A. M., Valera, J. L., & Doglioni, C. (2005). Subduction-related intermediate-depth and deep seismicity in Italy: Insights from thermal and rheological modeling. *Physics of the Earth and Planetary Interiors*, *149*(1-2), 65–79.
Catalano, R., Doglioni, C., & Merlini, S. (2001). On the Mesozoic Ionian Basin. *Geophysical Journal International*, *144*(1), 49–64.
Cernobori, L., Hirn, A., McBride, J. H., Nicolich, R., Petronio, L., Romanelli, M., & STREAMERS/PROFILES Working Groups (1996). Crustal image of the Ionian Basin and its Calabrian margins. *Tectonophysics*, *264*, 175–189.
Chertova, M. V., Spakman, W., Geenen, T., van den Berg, A. P., & van Hinsbergen, D. J. J. (2014). Underpinning tectonic reconstructions of the western Mediterranean region with dynamic slab evolution from 3-D numerical modeling. *Journal of Geophysical Research: Solid Earth*, *119*, 5876–5902. https://doi.org/10.1002/2014JB011150
Chiarabba, C., De Gori, P., & Speranza, F. (2008). The southern Tyrrhenian subduction zone: deep geometry, magmatism and Plio-Pleistocene evolution. *Earth and Planetary Science Letters*, *268*(3-4), 408–423.
Christensen, N. I., & Mooney, W. D. (1995). Seismic velocity structure and composition of the continental crust: A global view. *Journal of Geophysical Research*, *100*(B6), 9761–9788.
Cimini, G. B. (1999). P-wave deep velocity structure of the southern Tyrrhenian subduction zone from nonlinear teleseismic traveltime tomography. *Geophysical Research Letters*, *26*(24), 3709–3712.
Civello, S., & Margheriti, L. (2004). Toroidal mantle flow around the Calabrian slab (Italy) from SKS splitting. *Geophysical Research Letters*, *31*, L10601. https://doi.org/10.1029/2004GL019607
Cohen, J. K., & Stockwell Jr, J. W. (2000). CWP/SU: Seismic Unix Release 35: A free package for seismic research and processing. Centre for Wave Phenomenon, Colorado School of Mines.
Dannowski, A., Kopp, H., Klingelhoefer, F., Klaeschen, D., Gutscher, M. A., Krabbenhoeft, A., & Klaucke, I. (2019). Ionian Abyssal Plain: A window into the Tethys oceanic lithosphere. *Solid Earth*, *10*(2), 447–462.
de Voogd, B., Truffert, C., Chamot-Rooke, N., Huchon, P., Lallemant, S., & Le Pichon, X. (1992). Two-ship deep seismic soundings in the basins of the eastern Mediterranean Sea (Pasiphae cruise). *Geophysical Journal International*, *109*(3), 536–552.
Dellong, D., Klingelhoefer, F., Kopp, H., Graindorge, D., Margheriti, L., Moretti, M., et al. (2018). Crustal structure of the Ionian Basin and eastern Sicily margin: Results from a wide-angle seismic survey. *Journal of Geophysical Research: Solid Earth*, *123*, 2090–2114. https://doi.org/10.1002/2017JB015312
Engdahl, E. R., van der Hilst, R., & Buland, R. (1998). Global teleseismic earthquake relocation with improved travel times and procedures for depth determination. *Bulletin of the Seismological Society of America*, *88*(3), 722–743.
Faccenna, C., Funiciello, F., Giardini, D., & Lucente, P. (2001). Episodic back-arc extension during restricted mantle convection in the central Mediterranean. *Earth and Planetary Science Letters*, *187*(1-2), 105–116.
Faccenna, C., Molin, P., Orecchio, B., Olivetti, V., Bellier, O., Funiciello, F., et al. (2011). Topography of the Calabria subduction zone (southern Italy): Clues for the origin of Mt. Etna. *Tectonics*, *30*, TC1003. https://doi.org/10.1029/2010TC002694
Faccenna, C., Piromallo, C., Crespo-Blanc, A., Jolivet, L., & Rossetti, F. (2004). Lateral slab deformation and the origin of the western Mediterranean arcs. *Tectonics*, *23*, TC1012. https://doi.org/10.1029/2002TC001488

Ferranti, L., Monaco, C., Antonioli, F., Maschio, L., Kershaw, S., & Verrubbi, V. (2007). The contribution of regional uplift and coseismic slip to the vertical crustal motion in the Messina Straits, southern Italy: Evidence from raised Late Holocene shorelines. *Journal of Geophysical Research*, *112*, B06401. https://doi.org/10.1029/2006JB004473

Forte, A. M., Dziewonski, A. M., & Woodward, R. L. (1993). Aspherical structure of the mantle, tectonic plate motions, nonhydrostatic geoid, and topography of the core-mantle boundary. *Geophysical Monograph-American Geophysical Union*, *72*, 135–135.

Frizon de Lamotte, D., Raulin, C., Mouchot, N., Wrobel-Daveau, J. C., Blanpied, C., & Ringenbach, J. C. (2011). The southernmost margin of the Tethys realm during the Mesozoic and Cenozoic: Initial geometry and timing of the inversion processes. *Tectonics*, *30*, TC3002. https://doi.org/10.1029/2010TC002691

Funiciello, F., Moroni, M., Piromallo, C., Faccenna, C., Cenedese, A., & Bui, H. A. (2006). Mapping mantle flow during retreating subduction: Laboratory models analyzed by feature tracking. *Journal of Geophysical Research*, *111*, B03402. https://doi.org/10.1029/2005JB003792

Gallais, F., Gutscher, M. A., Graindorge, D., Chamot-Rooke, N., & Klaeschen, D. (2011). A Miocene tectonic inversion in the Ionian Sea (central Mediterranean): Evidence from multichannel seismic data. *Journal of Geophysical Research*, *116*, B12108. https://doi.org/10.1029/2011JB008505

Gallais, F., Gutscher, M.-A., Klaeschen, D., & Graindorge, D. (2012). Two-stage growth of the Calabrian accretionary wedge in the Ionian Sea (central Mediterranean): Constraints from depth migrated multi-channel seismic data. *Marine Geology*, *326-328*, 28–45. https://doi.org/10.1016/j.margeo.2012.08.006

Giacomuzzi, G., Civalleri, M., De Gori, P., & Chiarabba, C. (2012). A 3D Vs model of the upper mantle beneath Italy: Insight on the geodynamics of central Mediterranean. *Earth and Planetary Science Letters*, *335*, 105–120.

Govers, R., & Wortel, M. J. R. (2005). Lithosphere tearing at STEP faults: Response to edges of subduction zones. *Earth and Planetary Science Letters*, *236*(1-2), 505–523.

Gutscher, M.-A., Dominguez, S., Mercier de Lepinay, B., Pinheiro, L., Gallais, F., Babonneau, N., et al. (2016). Tectonic expression of an active slab tear from high-resolution seismic and bathymetric data offshore Sicily (Ionian Sea). *Tectonics*, *35*, 39–54. https://doi.org/10.1002/2015TC003898

Gutscher, M.-A., Dominguez, S., Westbrook, G., Le Roy, P., Rosas, F. M., Duarte, J. C., et al. (2012). The Gibraltar subduction: A decade of new geophysical data. *Tectonophysics*, *574-575*, 72–91. https://doi.org/10.1016/j.tecto.2012.08.038

Gutscher, M.-A., Dominguez, S., Westbrook, G. K., Gente, P., Babonneau, N., Mulder, T., et al., & the Delila and DelSis Scientific Teams (2009). Tectonic shortening and gravitational spreading in the Gulf of Cadiz accretionary wedge: Observations from multi-beam bathymetry and seismic profiling. Sp. Vol. on submarine instabilities. *Marine and Petroleum Geology*, *26*, 647–659. https://doi.org/10.1016/jmarpetgeo200711008

Gutscher, M.-A., Kopp, H., Krastel, S., Bohrmann, G., Garlan, T., Zaragosi, S., et al. (2017). Active tectonics of the Calabrian subduction revealed by new multi-beam bathymetric data and high-resolution seismic profiles in the Ionian Sea (central Mediterranean). *Earth and Planetary Science Letters.*, *461*, 61–72. https://doi.org/10.1016/j.epsl.2016.12.020

Gutscher, M.-A., Malod, J., Rehault, J.-P., Contrucci, I., Klingelhoefer, F., Mendes-Victor, L., & Spakman, W. (2002). Evidence for active subduction beneath Gibraltar. *Geology*, *30*, 1071–1074.

Gutscher, M.-A., Roger, J., Baptista, M. A., Miranda, J. M., & Tinti, S. (2006). The source of the 1693 Catania earthquake and tsunami (southern Italy): New evidence from tsunami modeling of a locked subduction fault plane. *Geophysical Research Letters*, *33*, L08309. https://doi.org/10.1029/2005GL025442

Handy, M. R., Schmid, S. M., Bousquet, R., Kissling, E., & Bernoulli, D. (2010). Reconciling plate-tectonic reconstructions of Alpine Tethys with the geological-geophysical record of spreading and subduction in the Alps. *Earth-Science Reviews*, *102*(3-4), 121–158.

Heit, B., Mancilla, F. D. L., Yuan, X., Morales, J., Stich, D., Martín, R., & Molina-Aguilera, A. (2017). Tearing of the mantle lithosphere along the intermediate-depth seismicity zone beneath the Gibraltar Arc: The onset of lithospheric delamination. *Geophysical Research Letters*, *44*, 4027–4035. https://doi.org/10.1002/2017GL073358

Heuret, A., & Lallemand, S. (2005). Plate motions, slab dynamics and back-arc deformation. *Physics of the Earth and Planetary Interiors*, *149*(1-2), 31–51.

Hirn, A., Nicolich, R., Gallart, J., Laigle, M., Cernobori, L., & ETNASEIS Scientific Group (1997). Roots of Etna volcano in faults of great earthquakes. *Earth and Planetary Science Letters*, *148*(1-2), 171–191.

Ike, T., Moore, G. F., Kuramoto, S. I., Park, J. O., Kaneda, Y., & Taira, A. (2008). Variations in sediment thickness and type along the northern Philippine Sea Plate at the Nankai Trough. *Island Arc*, *17*(3), 342–357.

Jacques, E., Monaco, C., Tapponnier, P., Tortorici, L., & Winter, T. (2001). Faulting and earthquake triggering during the 1783 Calabria seismic sequence. *Geophysical Journal International*, *147*(3), 499–516.

Jolivet, L., Faccenna, C., Agard, P., Frizon de Lamotte, D., Menant, A., Sternai, P., & Guillocheau, F. (2015). Neo-Tethys geodynamics and mantle convection: From extension to compression in Africa and a conceptual model for obduction. *Canadian Journal of Earth Sciences*, *53*(11), 1190–1204.

Kastens, K. A. (1991). Rate of outward growth of the Mediterranean Ridge accretionary complex. *Tectonophysics*, *199*(1), 25–50.

Klingelhoefer, F., Gutscher, M. A., Ladage, S., Dessa, J. X., Graindorge, D., Franke, D., et al. (2010). Limits of the seismogenic zone in the epicentral region of the 26 December 2004 great Sumatra-Andaman earthquake: Results from seismic refraction and wide-angle reflection surveys and thermal modeling. *Journal of Geophysical Research*, *115*, B01304. https://doi.org/10.1029/2009JB006569

Koulali, A., Ouazar, D., Tahayt, A., King, R. W., Vernant, P., Reilinger, R. E., et al. (2011). New GPS constrains on active deformation along the Africa-Iberia plate boundary. *Earth and Planetary Science Letters*, *308*(1), 211–217. https://doi.org/10.1016/j.epsl.2011.05.048

Krien, Y., & Fleitout, L. (2008). Gravity above subduction zones and forces controlling plate motions. *Journal of Geophysical Research*, *113*, B09407. https://doi.org/10.1029/2007JB005270

Lallemand, S., Heuret, A., & Boutelier, D. (2005). On the relationships between slab dip, back-arc stress, upper plate absolute motion, and crustal nature in subduction zones. *Geochemistry, Geophysics, Geosystems*, *6*, Q09006. https://doi.org/10.1029/2005GC000917

Le Meur, E., Virieux, J., & Podvin, P. (1997). Seismic tomography of the Gulf of Corinth: A comparison of methods.

Levitt, D. A., & Sandwell, D. T. (1995). Lithospheric bending at subduction zones based on depth soundings and satellite gravity. *Journal of Geophysical Research*, *100*(B1), 379–400.

Loureiro, A., Afilhado, A., Matias, L., Moulin, M., & Aslanian, D. (2016). Monte Carlo approach to assess the uncertainty of wide-angle layered models: Application to the Santos Basin, Brazil. *Tectonophysics*, *683*, 286–307.

Maesano, F. E., Tiberti, M. M., & Basili, R. (2017). The Calabrian Arc: Three-dimensional modeling of the subduction interface. *Scientific Reports*, *7*(1), 8887.

Makris, J., Nicolich, R., & Weigel, W. (1986). A seismic study in the western Ionian Sea. *Annales Geophysicae Series B-Terrestrial and Planetary Physics*, *4*(6), 665–678.
Marani, M. P., & Trua, T. (2002). Thermal constriction and slab tearing at the origin of a superinflated spreading ridge: Marsili volcano (Tyrrhenian Sea). *Journal of Geophysical Research*, *107*(B9), 2188. https://doi.org/10.1029/2001JB000285
Marotta, M. A., Spelta, E., & Rizzetto, C. (2006). Gravity signature of crustal subduction inferred from numerical modelling. *Geophysical Journal International*, *166*(2), 923–938.
Medaouri, M., Déverchère, J., Graindorge, D., Bracene, R., Badji, R., Ouabadi, A., et al. (2014). The transition from Alboran to Algerian basins (western Mediterranean Sea): Chronostratigraphy, deep crustal structure and tectonic evolution at the rear of a narrow slab rollback system. *Journal of Geodynamics*, *77*, 186–205.
Minelli, L., & Faccenna, C. (2010). Evolution of the Calabrian accretionary wedge (central Mediterranean). *Tectonics*, *29*, TC4004. https://doi.org/10.1029/2009TC002562
Moretti, I., & Royden, L. (1988). Deflection, gravity anomalies and tectonics of doubly subducted continental lithosphere: Adriatic and Ionian Seas. *Tectonics*, *7*(4), 875–893.
Mueller, R. D., Roest, W. R., Royer, J.-Y., Gahagan, L. M., & Sclater, J. G. (1997). Digital isochrons of the world's ocean floor. *Journal of Geophysical Research*, *102*, 3211–3214. https://doi.org/10.1029/96JB01781
Neri, G., Marotta, A. M., Orecchio, B., Presti, D., Totaro, C., Barzaghi, R., & Borghi, A. (2012). How lithospheric subduction changes along the Calabrian Arc in southern Italy: Geophysical evidences. *International Journal of Earth Sciences*, *101*(7), 1949–1969.
Neri, G., Orecchio, B., Totaro, C., Falcone, G., & Presti, D. (2009). Subduction beneath southern Italy close the ending: Results from seismic tomography. *Seismological Research Letters*, *80*(1), 63–70. https://doi.org/10.1785/gssrl.80.1.63
Nicolich, R., Laigle, M., Hirn, A., Cernobori, L., & Gallart, J. (2000). Crustal structure of the Ionian margin of Sicily: Etna volcano in the frame of regional evolution. *Tectonophysics*, *329*(1-4), 121–139.
Oleskevich, D. A., Hyndman, R. D., & Wang, K. (1999). The updip and downdip limits to great subduction earthquakes: Thermal and structural models of Cascadia, south Alaska, SW Japan, and Chile. *Journal of Geophysical Research*, *104*(B7), 14,965–14,991.
Palano, M., Ferranti, L., Monaco, C., Mattia, M., Aloisi, M., Bruno, V., et al. (2012). GPS velocity and strain fields in Sicily and southern Calabria, Italy: Updated geodetic constraints on tectonic block interaction in the central Mediterranean. *Journal of Geophysical Research*, *117*, B07401. https://doi.org/10.1029/2012JB009254
Palano, M., Gonzalez, P. J., & Fernandez, J. (2015). The diffuse plate boundary of Nubia and Iberia in the western Mediterranean: Crustal deformation evidence for viscous coupling and fragmented lithosphere. *Earth and Planetary Science Letters*, *430*, 439–447. https://doi.org/10.1016/j.epsl.2015.08.040
Palano, M., Piromallo, C., & Chiarabba, C. (2017). Surface imprint of toroidal flow at retreating slab edges: The first geodetic evidence in the Calabrian subduction system. *Geophysical Research Letters*, *44*, 845–853. https://doi.org/10.1002/2016GL071452
Pavlis, N. K., Holmes, S. A., Kenyon, S. C., & Factor, J. K. (2012). The development and evaluation of the Earth Gravitational Model 2008 (EGM2008). *Journal of Geophysical Research*, *117*, B04406. https://doi.org/10.1029/2011JB008916
Piana Agostinetti, N., Steckler, M. S., & Lucente, F. P. (2009). Imaging the subducted slab under the Calabrian Arc, Italy, from receiver function analysis. *Lithosphere*, *1*(3), 131–138.
Piatanesi, A., & Tinti, S. (1998). A revision of the 1693 eastern Sicily earthquake and tsunami. *Journal of Geophysical Research*, *103*(B2), 2749–2758.
Polonia, A., Torelli, L., Mussoni, P., Gasperini, L., Artoni, A., & Klaeschen, D. (2011). The Calabrian Arc subduction complex in the Ionian Sea: Regional architecture, active deformation, and seismic hazard. *Tectonics*, *30*, TC5018. https://doi.org/10.1029/2010TC002821
Rosenbaum, G., Lister, G. S., & Duboz, C. (2002). Reconstruction of the tectonic evolution of the western Mediterranean since the Oligocene. *Journal of the Virtual Explorer*, *8*, 107–130.
Sallarès, V., Gailler, A., Gutscher, M.-A., Graindorge, D., Bartolomé, R., Gracia, E., et al. (2011). Seismic evidence for the presence of Jurassic oceanic crust in the central Gulf of Cadiz (SW Iberia margin). *Earth and Planetary Science Letters*, *311*(1-2), 112–123. https://doi.org/10.1016/j.epsl.2011.09.003
Sarkar, A., Nunn, J. A., & Hanor, J. S. (1995). Free thermohaline convection beneath allochthonous salt sheets: An agent for salt dissolution and fluid flow in Gulf Coast sediments. *Journal of Geophysical Research*, *100*(B9), 18,085–18,092.
Scarfì, L., Barberi, G., Barreca, G., Cannavò, F., Koulakov, I., & Patanè, D. (2018). Slab narrowing in the Central Mediterranean: the Calabro-Ionian subduction zone as imaged by high resolution seismic tomography. *Scientific Reports*, *8*(1), 5178. https://doi.org/10.1038/s41598-018-23543-8
Scarfì, L., Barberi, G., Musumeci, C., & Patanè, D. (2016). Seismotectonics of northeastern Sicily and southern Calabria (Italy): New constraints on the tectonic structures featuring in a crucial sector for the central Mediterranean geodynamics. *Tectonics*, *35*, 812–832. https://doi.org/10.1002/2015TC004022
Scarfì, L., Messina, A., & Cassisi, C. (2013). Sicily and southern Calabria focal mechanism database: A valuable tool for local and regional stress-field determination. *Annals of Geophysics*, *56*(1), 109.
Scarpa, R. (1982). Travel-time residuals and three-dimensional velocity structure of Italy. *Pure and Applied Geophysics*, *120*(3), 583–606.
Schellart, W. P. (2004). Kinematics of subduction and subduction-induced flow in the upper mantle. *Journal of Geophysical Research*, *109*, B07401. https://doi.org/10.1029/2004JB002970
Selvaggi, G., & Chiarabba, C. (1995). Seismicity and P-wave velocity image of the southern Tyrrhenian subduction zone. *Geophysical Journal International*, *121*(3), 818–826.
Séranne, M. (1999). The Gulf of Lion continental margin (NW Mediterranean) revisited by IBS: An overview. *Geological Society, London, Special Publications*, *156*(1), 15–36.
Song, T. R. A., & Simons, M. (2003). Large trench-parallel gravity variations predict seismogenic behavior in subduction zones. *Science*, *301*(5633), 630–633.
Spakman, W., van der Lee, S., & van der Hilst, R. (1993). Travel-time tomography of the European-Mediterranean mantle down to 1400 km. *Physics of the Earth and Planetary Interiors*, *79*(1-2), 3–74.
Spakman, W., & Wortel, R. (2004). A tomographic view on western Mediterranean geodynamics. In *The TRANSMED Atlas. The Mediterranean Region from Crust to Mantle* (pp. 31–52). Berlin, Heidelberg: Springer.
Speranza, F., Maniscalco, R., & Grasso, M. (2003). Pattern of orogenic rotations in central-eastern Sicily: Implications for the timing of spreading in the Tyrrhenian Sea. *Journal of the Geological Society*, *160*(2), 183–195.
Speranza, F., Minelli, L., Pignatelli, A., & Chiappini, M. (2012). The Ionian Sea: The oldest in situ ocean fragment of the world? *Journal of Geophysical Research*, *117*, B12101. https://doi.org/10.1029/2012JB009475

Underwood, M. B. (2007). Sediment inputs to subduction zones: Why lithostratigraphy and clay mineralogy matter. The Seismogenic Zone of Subduction Thrust Faults.
van Hinsbergen, D. J. J., Mensink, M., Langereis, C. G., Maffione, M., Spalluto, L., Tropeano, M., & Sabato, L. (2014). Did Adria rotate relative to Africa? *Solid Earth*, *5*(2), 611–629.
van Hinsbergen, D. J. J., Vissers, R. L. M., & Spakman, W. (2014). Origin and consequences of western Mediterranean subduction, rollback, and slab segmentation. *Tectonics*, *33*, 393–419. https://doi.org/10.1002/tect.20125
Watts, A. B., Platt, J. P., & Buhl, P. (1993). Tectonic evolution of the Alboran Sea basin. *Basin Research*, *5*, 153–177. https://doi.org/10.1111/j.1365-2117.1993.tb00063.x
Westaway, R. (1993). Quaternary uplift of southern Italy. *Journal of Geophysical Research*, *98*(B12), 21,741–21,772.
White, R. S., McKenzie, D., & O'Nions, R. K. (1992). Oceanic crustal thickness from seismic measurements and rare earth element inversions. *Journal of Geophysical Research*, *97*(B13), 19,683–19,715.
Wortel, M. J. R., & Spakman, W. (2000). Subduction and slab detachment in the Mediterranean-Carpathian region. *Science*, *290*(5498), 1910–1917. https://doi.org/10.1126/science.290.5498.1910
Wortel, R., Govers, R., & Spakman, W. (2009). Continental collision and the STEP-wise evolution of convergent plate boundaries: From structure to dynamics. In *Subduction Zone Geodynamics*, (pp. 47–59). Berlin, Heidelberg: Springer.
Zelt, C. A. (1999). Modeling strategies and model assessment for wide-angle seismic traveltime data. *Geophysical Journal International*, *139*(1), 183–204.
Zelt, C. A., & Smith, R. B. (1992). Seismic traveltime inversion for 2-D crustal velocity structure. *Geophysical Journal International*, *108*(1), 16–34.
Zito, G., Mongelli, F., De Lorenzo, S., & Doglioni, C. (2003). Heat flow and geodynamics in the Tyrrhenian Sea. *Terra Nova*, *15*(6), 425–432.

References From the Supporting Information

Brocher, T. M. (2005). Empirical relations between elastic wavespeeds and density in the Earth's crust. *Bulletin of the Seismological Society of America*, *95*(6), 2081–2092.
Casalbore, D., Ridente, D., Bosman, A., & Chiocci, F. L. (2017). Depositional and erosional bedforms in Late Pleistocene-Holocene prodelta deposits of the Gulf of Patti (southern Tyrrhenian margin, Italy). *Marine Geology*, *385*, 216–227.
Ludwig, W. J., Nafe, J. E., & Drake, C. L. (1970). The Sea, Vol. 4, Part 1.
Schmidt, S., Plonka, C., Gotze, H. J., & Lahmeyer, B. (2011). Hybrid modelling of gravity, gravity gradients and magnetic fields. *Geophysical Prospecting*, *59*(6), 1046–1051.